Nrf2 遺伝子ノックアウトマウスを用いた口腔病変のストレス応答の解析

課題番号　12671924

平成12年度～平成14年度科学研究費補助金（基盤研究C（2））

研究成果報告書

平成15年5月

研究代表者　柳　川　　徹

（筑波大学臨床医学系）

研究組織

研究代表者　柳川　徹（筑波大学臨床医学系）

研究分担者　石井 哲郎（筑波大学社会医学系）

交付決定額（配分額）　　（金額単位：千円）

	直接経費	間接経費	合計
平成 12 年度	1500	0	1500
平成 13 年度	900	0	900
平成 14 年度	900	0	900
総計	3300	0	3300

研究発表

（１）学会誌等

1) Ishii T, Itoh K, Takahashi S, Sato H, Yanagawa T, Katoh Y, Bannai S, Yamamoto M.
Transcription factor Nrf2 coordinately regulates a group of oxidative stress-inducible genes in macrophages. J Biol Chem. 2000 May 26;275(21):16023-9.

2) Ishii T, Itoh K, Akasaka J, Yanagawa T, Takahashi S, Yoshida H, Bannai S, Yamamoto M.
Induction of murine intestinal and hepatic peroxiredoxin MSP23 by dietary butylated hydroxyanisole. Carcinogenesis. 2000 May;21(5):1013-6.

3) Yanagawa T, Itoh K, Yamaguchi A, Shibata Y, Sano T, Takahashi S, Ishii T, Yoshida H, and Yamamoto M.
Disruption of nrf2 gene causes tooth decolorization: involvment of iron transport disorder（投稿準備中）

（２）口頭発表

1) 柳川徹　鬼澤浩司郎、遊佐浩　吉田廣、山口朗
Nrf2 ノックアウトマウスにおける上顎前歯の色調の変化
第 55 回日本口腔科学会 4 月 26-27 日 2001 年　盛岡

2) Tetsuro Ishii, Toru Yanagawa, and Ken Itoh,
Enhanced Expression of Multiubiquitin-binding Protein A170 by Stress in Murine Macrophage.　2002 Ubiquitin Meeting August11-14, 2002 coloradosprings

（３）出版物

なし

研究成果による工業所有権の出願・取得状況

なし

Carcinogenesis vol.21 no.5 pp.1013–1016, 2000

Induction of murine intestinal and hepatic peroxiredoxin MSP23 by dietary butylated hydroxyanisole

Tetsuro Ishii[3], Ken Itoh, Junetsu Akasaka, Toru Yanagawa[2], Satoru Takahashi[1], Hiroshi Yoshida[2], Shiro Bannai and Masayuki Yamamoto[1]

Department of Biochemistry, Institute of Basic Medical Sciences, [1]Tsukuba Advanced Research Alliance Center and [2]Department of Oral and Maxillofacial Surgery, Institute of Clinical Sciences, University of Tsukuba, 1-1-1 Tennoudai, Tsukuba, Ibaraki 305-8575, Japan

[3]To whom correspondence should be addressed
Email: teishii@md.tsukuba.ac.jp

Feeding mice with 2(3)-*t*-butyl-4-hydroxyanisole (BHA) induces phase II detoxifying enzymes that inhibit the action of carcinogens. We have found that dietary BHA induces intestinal and hepatic MSP23 (also called peroxiredoxin I), a stress-inducible antioxidant, in a manner similar to the induction of glutathione *S*-transferases (GSTs). The levels of MSP23 in the proximal intestine and liver, estimated by immunoblotting, increased approximately 1.9- and 1.3-fold, respectively, in mice fed a diet containing 0.7% (w/w) BHA for 7 days. The level of MSP23 mRNA in these tissues also increased more than 2-fold after mice were fed BHA, suggesting that the induction of MSP23 is controlled at the transcription level. Immunostaining of the small intestine shows that MSP23 is expressed mainly in the columnar epithelial cells. The induction of MSP23 may be important to protect the cells and tissues against toxic electrophiles and reactive oxygen species.

Introduction

2(3)-*t*-Butyl-4-hydroxyanisole (BHA) is a synthetic phenolic antioxidant that is widely used as a food preservative. Dietary administration of BHA protects animals against various carcinogens (1), presumably through the induction of phase II enzymes that detoxify the activated electrophilic metabolites of carcinogens. In the murine liver and intestine, BHA markedly induces the expression of glutathione *S*-transferases (GSTs) (2), NAD(P)H:quinone reductase (3), UDP-glucuronosyltransferases (4) and epoxide hydrolases (5).

A 23 kDa oxidative stress-inducible protein termed MSP23, which is now classified as murine peroxiredoxin (Prx) I, was first cloned in macrophages by differential screening using diethylmaleate, a sulfhydryl-reactive electrophilic agent, as inducer (6). MSP23 is ubiquitously expressed and its levels are especially high in the liver (6). The peroxiredoxin proteins have conserved cysteine residues that participate in oxidoreductive reactions and protect macromolecules from oxidative damage (7). The mammalian Prx proteins I–III reduce hydrogen peroxide generated in response to growth factors and tumor necrosis factor-α (TFN-α) in the presence of the thioredoxin/thioredoxin reductase system (8,9). Prx I and II regulate the activation of NF-κB (10) and AP-1 (11) and protect cells from apoptosis by reducing oxidative damage (12).

Since the BHA metabolite *t*-butylhydroquinone induced MSP23 in murine macrophages *in vitro*, we examined the effect of dietary BHA on the expression of MSP23 in mouse tissues. In this study we show that dietary BHA leads to induction of MSP23 in the small intestine and liver. The induction of MSP23 may be important in protecting the tissues from oxidative damage.

Abbreviations: BHA, 2(3)-*t*-butyl-4-hydroxyanisole; GST, glutathione *S*-transferase; Prx, peroxiredoxin; TNF-α, tumor necrosis factor-α.

Materials and methods

Treatment of animals

Female ICR mice (Charles River Co.) between 8 and 12 weeks of age were used. Mice of each genotype were randomly assigned to two groups. Both groups were fed either the basal powder diet (MF; Oriental Yeast Co.) or the experimental diet, which was prepared by supplementing the food with BHA at a concentration of 0.7% (w/w) as described previously (13). During the experiment, the mice had free access to food and tap water. After 1–14 days the animals were killed by decapitation. All animal experiments were carried out after receiving permission from the Animal Experiment Committee, University of Tsukuba, and in accordance with the University of Tsukuba's Regulations on Animal Experiments and Japanese Governmental Law No. 105.

Tissue preparation

The tissues were excised immediately after death. The intestine between the stomach and the colon was dissected into 5 cm segments and each segment was cut open and washed with ice-cold phosphate-buffered saline. Aliquots (15 mg wet wt) of washed tissues were homogenized in small glass homogenizers in 1 ml SDS sample buffer (2% w/v SDS, 10% v/v glycerol, 2 mM EDTA, 1 mM phenylmethylsulfonyl fluoride, 50 mM Tris–HCl, pH 6.8), boiled for 5 min and stored at –20°C until use. The protein content of tissue homogenates was determined using BCA reagent (Pierce). Samples were mixed with bromophenol blue and 2-mercaptoethanol and boiled for 5 min, then immediately subjected to SDS–PAGE (10% w/v acrylamide). Western blots were visualized using ECL reagent (Amersham). MSP23 was detected with polyclonal rabbit antiserum raised against rat Prx I purified from rat liver (14). Immunostained protein bands were quantified by densitometric analysis using the NIH Image program. Proteins that partially remained in the gels after electrotransfer were stained with Coomassie brilliant blue R 250 (Fluka) to detect the induction of GSTs.

Immunohistological staining

Immunostaining of tissues was performed by the horseradish peroxidase-conjugated streptavidin biotin method (LsAB method; Nichirei) following the manufacturer's protocol. Pieces of proximal intestine were washed in phosphate-buffered saline, then post-fixed with 4% paraformaldehyde for 3 h and embedded in paraffin. The sections were incubated with 1:1000 (v/v) diluted anti-Prx I rabbit antiserum at 4°C overnight. The antigen was stained brownish red. The sections were counterstained with hematoxylin.

Results

To examine the effects of dietary BHA on the expression levels of MSP23 in tissues, we fed wild-type ICR female mice a diet containing 0.7% BHA for up to 2 weeks and monitored the level of MSP23. Using anti-Prx I antiserum, we detected a single 23 kDa immunostained band corresponding to MSP23 in both intestine and liver from control and BHA-fed mice. The induction efficiency of dietary BHA was monitored by detecting the induced protein bands of α and μ class GSTs in the intestine (Figure 1, upper) and π class GST in the liver, which have apparent masses of ~25 kDa (13). We found that

MSP23 was measurably increased in the small intestine after 5 days of continuous BHA treatment and reached a maximum level after 7 days, which lasted for at least 1 week (Figure 1, lower). This time course indicated that the induction of intestinal MSP23 by dietary BHA is significantly slower than that of the GSTs. To examine the location of the induced MSP23 in the intestinal duct, we dissected the small intestine (mean length ± SD = 47.5 ± 2.1 cm, n = 5) into nine or 10 5 cm segments and monitored the relative levels of MSP23 in each segment. The inducing effect of BHA was most evident in the proximal to middle part of the small intestine (Figure 2, lanes 2–10) and was not significant in either the stomach or the colon (Figure 2, lanes 1 and 11). After treatment with BHA for 7 days, the levels of intestinal and hepatic MSP23 were enhanced 1.92 ± 0.39- and 1.25 ± 0.21-fold (mean ± SD, n = 6), respectively (Figure 3). The inducing effect was statistically significant ($P < 0.001$ in intestine and $P < 0.05$ in liver). The ratio of intestinal to hepatic MSP23 levels in mice fed the normal diet was calculated to be 0.58 (mean of six mice), which increased to 0.89 after treatment with BHA (Figure 3).

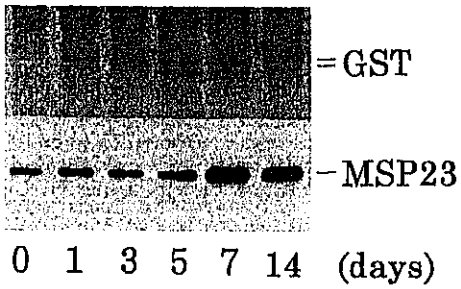

Fig. 1. Time-dependent induction of MSP23 in the small intestine by dietary BHA. Induction of α and μ class GSTs is visible as stained protein bands with masses of ~25 kDa (upper). The immunostained MSP23 band (lower) is shown during the time of continuous BHA feeding. Number of days refers to after BHA was added to the diet.

We next examined the effect of dietary BHA on the levels of MSP23 mRNA (1.0 kb) in the proximal intestine and liver by northern blotting, We found that it enhanced the MSP23 mRNA levels 2.30 ± 0.72- and 1.82 ± 0.08-fold (mean ± SD, n = 4 and 6), respectively (Figure 4). The inducing effect of dietary BHA was statistically significant ($P < 0.001$ in both intestine and liver). The effect of dietary BHA on the levels of MSP23 mRNA was roughly parallel to the effect on the levels of MSP23 protein in both tissues (compare Figure 4 with Figure 2). These results suggest that the induction of MSP23 by dietary BHA in these tissues is regulated at the transcriptional level.

To examine the localization of MSP23 in the proximal small intestine, a histochemical study was performed using antibody staining with an anti-Prx I antiserum (Figure 5). In the intestine, heavy staining was seen in the columnar epithelial cells, especially those located in the middle to lower part of the intestinal villi. In contrast, only slight staining was seen in the Paneth cells, myofibroblasts, goblet cells and muscularis mucosae (Figure 5). The location of staining of MSP23 in the intestine was fundamentally the same, but the intensity appeared higher after mice were fed BHA (compare Figure 5a with b).

Discussion

We have shown for the first time that: (i) dietary BHA induces intestinal and hepatic MSP23 in mice (Figures 1–4); (ii) MSP23 is mainly expressed in columnar intestinal epithelial cells facing the lumen of the ducts (Figure 5). Notably, dietary BHA almost doubled the level of intestinal MSP23 and the enhanced level approached that of the liver, which expressed the highest MSP23 level among the major tissues. No induction of MSP23 by dietary BHA could be detected in the stomach and colon (Figure 2) or in brain, heart, lung, spleen and kidney (not shown) by immunoblotting. Thus, the induction of MSP23 by dietary BHA appears specific to intestine and liver.

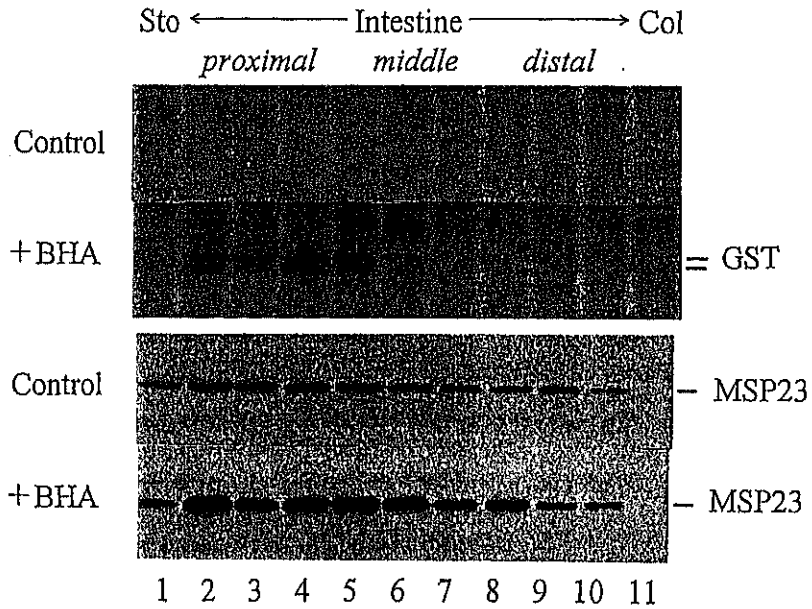

Fig. 2. Locus of induction of MSP23 in small intestine. The small intestines of mice fed a diet without (control) or with BHA treatment (+BHA) were cut into 5 cm pieces (lanes 2–10, proximal–middle–distal) from the stomach (lane 1) to the colon (lane 11). The dye stained gel (upper) and the bands immunostained with anti-MSP23 antibodies (lower) are shown.

The administration of BHA or other antioxidants to rodents subsequently induces specific activities of enzymes in the liver and peripheral tissues of these animals (15). These enzymes include GST (2), NAD(P)H:quinone reductase (3), UDP-glucuronosyltransferase (4), microsomal epoxide hydrolase (5), aflatoxin B1 aldehyde reductase (16), glucose 6-phosphate dehydrogenase (17) and γ-glutamylcysteine synthetase (18). The increased levels of these enzymes reduce the susceptibility of cells to higher concentrations of toxic electrophilic compounds and carcinogens. This protective metabolic response provoked by BHA and other agents has been called an 'electrophile counterattack' (19). This study indicates that the

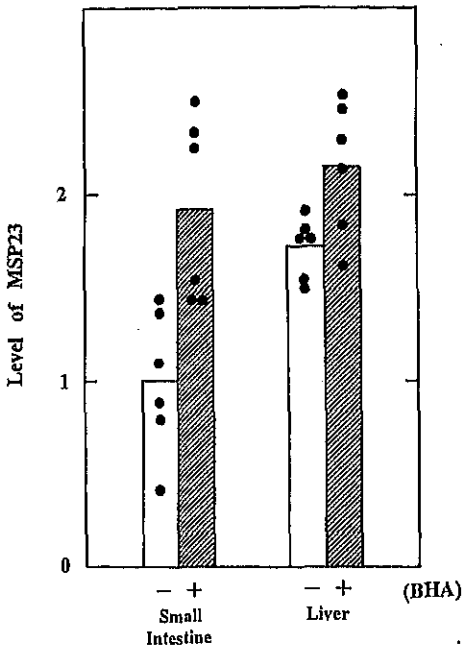

Fig. 3. Densitometric analysis of the effect of dietary BHA on the levels of MSP23 in small intestine and liver. Mice were fed a diet with or without BHA for 7 days. The mean values of the level of MSP23 in the proximal small intestine of control mice were defined as the standard (1.00). Each dot represents the relative value of MSP23 in each mouse.

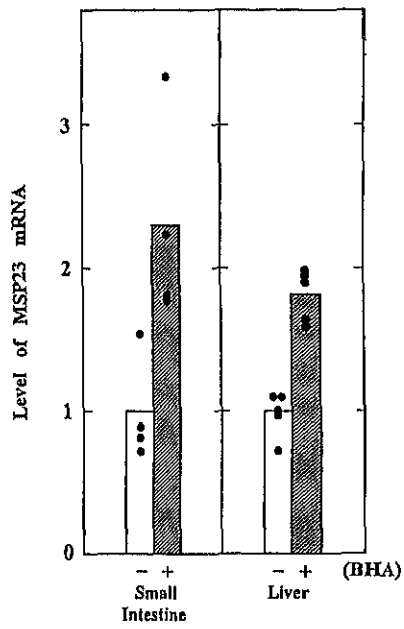

Fig. 4. Induction of intestinal and hepatic MSP23 mRNA by dietary BHA. Densitometric analysis of MSP23 mRNA levels in the proximal small intestine (left) and liver (right). The mean values of the level of MSP23 mRNA in the small intestine and liver of control mice were defined as the standard (1.00). The relative values were calculated using β-actin mRNA (2.0 kb) as an internal standard.

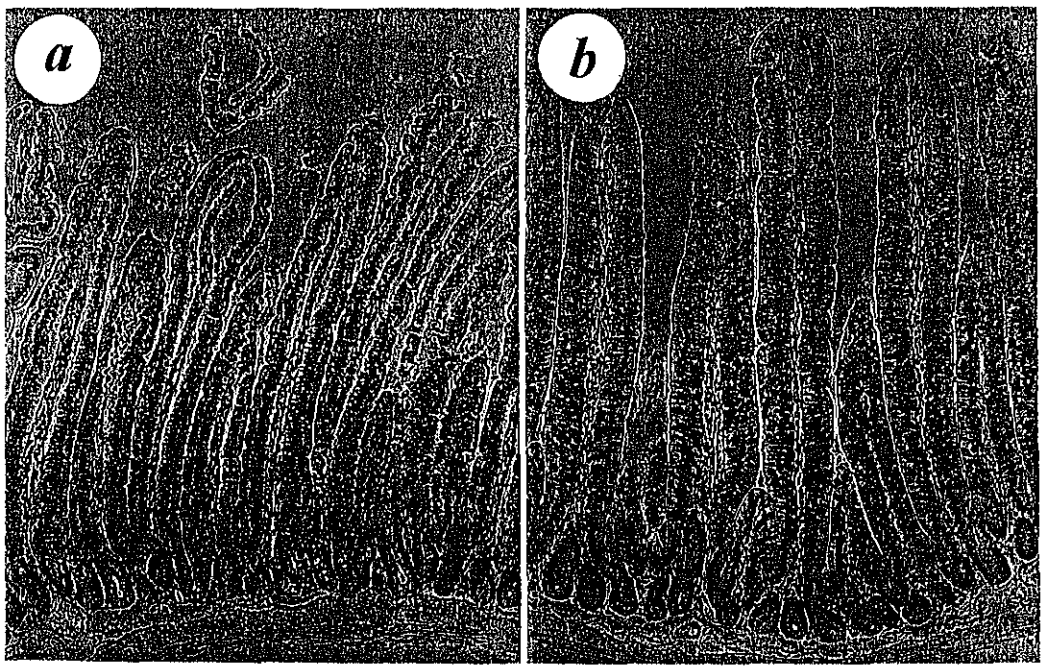

Fig. 5. Localization of MSP23 in proximal intestine. MSP23 (brownish red) was immunostained with antiserum as described in Materials and methods. (a) Control. (b) BHA fed. ×370 magnification.

induction of MSP23, in addition to phase II enzymes, is one of the important adaptive responses induced by dietary BHA. We have no experimental results that explain the reason for the delayed induction of MSP23 compared with that of GST by dietary BHA. One possibility to explain this phenomenon is that dietary BHA gradually causes oxidative damage and that accumulated damage induces MSP23. Another possibility is that MSP23 mRNA is induced early after BHA treatment but that the apparent MSP23 protein level increased later because the protein degradation rate was enhanced in the early stages following treatment. Further precise analysis is necessary to elucidate the delayed induction of MSP23 by dietary BHA.

MSP23 is an oxidative stress-inducible protein belonging to the peroxiredoxin family. Members of this family have the ability to reduce hydrogen peroxide in the presence of the thioredoxin system (10) and to trap thiyl radicals with reactive cysteine residues (8). Transient expression of Prx I or II inhibited activation of NF-κB by extracellularly added H_2O_2 or TNF-α (10), although the level of induced Prx I in NIH 3T3 cells appeared to be less than 2-fold. It has also been shown that overexpression of Prx II in endothelial cells significantly blocks TNF-α-induced AP-1 activation (11). These results indicate that Prx enzymes play an important role in eliminating peroxides generated during metabolism. Therefore, the enhanced MSP23 level in mouse tissues induced by dietary BHA probably contributes to a reduction in cellular damage by oxidants. Although BHA is known as an antioxidant, it is oxidatively demethylated in mammalian tissues to *t*-butylhydroquinone. This metabolite is autoxidized to *t*-butylquinone and may produce reactive oxygen species by redox cycling (20). Using the EPR spin trapping technique, the generation of hydroxy radicals by autoxidation of *t*-butylhydroquinone to *t*-butylquinone was detected in human hepatoma HepG2 cells (21). There is a correlation between production of oxygen radicals and the induction of GST Ya gene expression (22). We observed that *t*-butylquinone supplementation of the culture medium markedly induced MSP23 in murine peritoneal macrophages (unpublished data). BHA, however, only slightly induced MSP23 in these cells. Therefore, BHA has the potential to act as both oxidant and antioxidant, and the generated quinone and/or oxygen radicals may induce phase II enzymes (23) and MSP23.

In conclusion, the present study demonstrates that the induction of MSP23 (Prx I) in intestine and liver is one of the broad defense reactions provoked by dietary BHA. These results suggest that MSP23 plays an important role in protecting these tissues against toxic electrophiles and reactive oxygen species.

Acknowledgements

This work was supported in part by Grants-in-Aid from the Ministry of Education, Science, Sports and Culture of Japan, Research for the Future of the Japanese Society for Promotion of Science (JSPS) and the JSPS. K.I. is a research fellow of the JSPS.

References

1. Wattenberg,L.W. (1972) Inhibition of carcinogenic and toxic effects of polycyclic hydrocarbons by phenolic antioxidants and ethoxyquin. *J. Natl Cancer Inst.*, 48, 1425–1430.
2. Benson,A.M., Batzinger,R.P., Ou,S.-Y.L., Bueding,E., Cha,Y.-N. and Talalay,P. (1978) Elevation of hepatic glutathione *S*-transferase activities and protection against mutagenic metabolites of benzo(a)pyrene by dietary antioxidants. *Cancer Res.*, 38, 4486–4495.
3. Benson,A.M., Hunkeler,M.J. and Talalay,P. (1980) Increase of NAD(P)H:quinone reductase by dietary antioxidants: possible role in protection against carcinogenesis and toxicity. *Proc. Natl Acad. Sci. USA*, 77, 5216–5220.
4. Moldeus,P., Dock,L., Cha,Y.-N., Berggren,M. and Jernstrom,B. (1982) Elevation of conjugation capacity in isolated hepatocytes from BHA-treated mice. *Biochem. Pharmacol.*, 31, 1907–1910.
5. Cha,Y.-N., Martz,F. and Beuding,E. (1978) Enhancement of liver microsome epoxide hydratase activity in rodents by treatment with 2(3)-*tert*-butyl-4-hydroxyanisole. *Cancer Res.*, 38, 4496–4498.
6. Ishii,T., Yamada,M., Sato,H., Matsue,M., Taketani,S., Nakayama,K., Sugita,Y. and Bannai,S. (1993) Cloning and characterization of a 23-kDa stress-induced mouse peritoneal macrophage protein. *J. Biol. Chem.*, 268, 18633–18636.
7. Yim,M.B., Chae,H.Z., Rhee,S.G., Chock,P.B. and Stadtman,E.R. (1994) On the protective mechanism of the thiol-specific antioxidant enzyme against the oxidative damage of biomacromolecules. *J. Biol. Chem.*, 269, 1621–1626.
8. Chae,H.Z., Chung,S.J. and Rhee,S.G. (1994) Thioredoxin-dependent peroxide reductase from yeast. *J. Biol. Chem.*, 269, 27670–27678.
9. Kang,S.W., Chae,H.Z., Seo,M.S., Kim,K., Baines,I.C. and Rhee,S.G. (1998) Mammalian peroxiredoxin isoforms can reduce hydrogen peroxide generated in response to growth factors and tumor necrosis factor-α. *J. Biol. Chem.*, 273, 6297–6302.
10. Jin,D.-Y., Chae,H.Z., Rhee,S.G. and Jeang,K.-T. (1997) Regulatory role for a novel human thioredoxin peroxidase in NF-κB activation. *J. Biol. Chem.*, 272, 30952–30961.
11. Shau,H., Huang,A.C., Faris,M., Nazarian,R., de Vellis,J. and Chen,W. (1998) Thioredoxin peroxidase (natural killer enhancing factor) regulation of activator protein-1 function in endothelial cells. *Biochem. Biophys. Res. Commun.*, 249, 682–686.
12. Zhang,P., Liu,B. Kang,S.W., Seo,M.S., Rhee,S.G. and Obeid,L.M. (1997) Thioredoxin peroxidase is a novel inhibitor of apoptosis with a mechanism distinct from that of Bcl-2. *J. Biol. Chem.*, 272, 30615–30618.
13. Itoh,K., Chiba,T., Takahashi,S., Ishii,T., Igarashi,K., Katoh,Y., Oyake,T., Hayashi,N., Satoh,K., Hatayama,I., Yamamoto,M. and Nabeshima,Y. (1997) An Nrf2/small Maf heterodimer mediates the induction of phase II detoxifying enzyme genes through antioxidant response elements. *Biochem. Biophys. Res. Commun.*, 236, 313–322.
14. Ishii,T., Kawane,T., Taketani,S. and Bannai,S. (1995) Inhibition of the thiol-specific antioxidant activity of rat liver MSP23 protein by hemin. *Biochem. Biophys. Res. Commun.*, 216, 970–975.
15. Primiano,T., Sutter,T.R. and Kensler,T.W. (1997) Antioxidant-inducible genes. *Adv. Pharmacol.*, 38, 293–328.
16. Ellis,E.M., Judah,D.J., Neal,G.E. and Hayes,J.D. (1993) An ethoxyquin-inducible aldehyde reductase from rat liver that metabolizes aflatoxin B1 defines a sub-family of aldo-keto reductase. *Proc. Natl Acad. Sci. USA*, 90, 10350–10354.
17. Cha,Y.-N. and Bueding,E. (1979) Effect of 2(3)-*tert*-butyl-4-hydroxyanisole (BHA) administration on the activities of several hepatic microsomal and cytoplasmic enzymes in mice. *Biochem. Pharmacol.*, 28, 1917–1921.
18. Eaton,D.L. and Hamel,D.M. (1994) Increase in γ-glutamylcysteine synthetase activity as a mechanism for butylated hydroxyanisole-mediated elevation of hepatic glutathione. *Toxicol. Appl. Pharmacol.*, 126, 145–149.
19. Prestera,T., Zhang,Y., Spencer,S.R., Wilczak,C.A. and Talalay,P. (1993) The electrophile counterattack response: protection against neoplasia and toxicity. *Adv. Enzyme. Regul.*, 33, 281–296.
20. Kahl,R., Weinke,S. and Kappus,H. (1989) Production of reactive oxygen species due to metabolic activation of butylated hydroxyanisole. *Toxicology*, 59, 179–194.
21. Pinkus,R., Weiner,M. and Daniel,V. (1996) Role of oxidants and antioxidants in the induction of AP-1, NF-κB and glutathione *S*-transferase gene expression. *J. Biol. Chem.*, 271, 13422–13429.
22. Pinkus,R., Weiner,L.M. and Daniel,V. (1995) Role of quinone-mediated generation of hydroxyl radicals in the induction of glutathione S-transferase gene expression. *Biochemistry*, 34, 81–88.
23. Yu,R., Tan,T.-H. and Kong,A.-N.T. (1997) Butylated hydroxyanisole and its metabolite *tert*-butylhydroquinone differentially regulate mitogen-activated protein kinases: the role of oxidative stress in the activation of mitogen-activated protein kinases by phenolic antioxidants. *J. Biol. Chem.*, 272, 28962–28970.

Received August 17, 1999; revised December 30, 1999; accepted January 5, 2000

THE JOURNAL OF BIOLOGICAL CHEMISTRY
Vol. 275, No. 21, Issue of May 26, pp. 16023–16029, 2000
Printed in U.S.A.

Transcription Factor Nrf2 Coordinately Regulates a Group of Oxidative Stress-inducible Genes in Macrophages*

Received for publication, September 10, 1999, and in revised form, January 19, 2000

Tetsuro Ishii‡, Ken Itoh‡§, Satoru Takahashi, Hideyo Sato, Toru Yanagawa, Yasutake Katoh, Shiro Bannai, and Masayuki Yamamoto¶

From the Institute of Basic Medical Sciences and Center for Tsukuba Advanced Research Alliance, University of Tsukuba, 1-1-1 Tennoudai, Tsukuba 305-8577, Japan

Electrophiles and reactive oxygen species have been implicated in the pathogenesis of many diseases. Transcription factor Nrf2 was recently identified as a general regulator of one defense mechanism against such havoc. Nrf2 regulates the inducible expression of a group of detoxication enzymes, such as glutathione *S*-transferase and NAD(P)H:quinone oxidoreductase, via antioxidant response elements. Using peritoneal macrophages from Nrf2-deficient mice, we show here that Nrf2 also controls the expression of a group of electrophile- and oxidative stress-inducible proteins and activities, which includes heme oxygenase-1, A170, peroxiredoxin MSP23, and cystine membrane transport (system x_c^-) activity. The response to electrophilic and reactive oxygen species-producing agents was profoundly impaired in Nrf2-deficient cells. The lack of induction of system x_c^- activity resulted in the minimum level of intracellular glutathione, and Nrf2-deficient cells were more sensitive to toxic electrophiles. Several stress agents induced the DNA binding activity of Nrf2 in the nucleus without increasing its mRNA level. Thus Nrf2 regulates a wide-ranging metabolic response to oxidative stress.

Oxidative stress conditions or enhanced production of reactive oxygen species (ROS)[1] result from a variety of stimuli including ionizing radiation, exposure to xenobiotics, inflammation, and phagocytosis (1). Treatment of mammalian cells with electrophilic agents usually provokes cellular responses, including transcriptional activation of genes encoding proteins that partake in the defense against oxidative stress. This process is referred to as the electrophile counterattack response (2). Through analyses of mouse and rat glutathione *S*-transferase (GST) Ya subunit genes and the rat NAD(P)H:quinone oxidoreductase (NQO1) subunit gene, the *cis*-acting element responsible for the induction by electrophiles was independently identified as an electrophile-responsive element (EpRE) (3) or antioxidant-responsive element (ARE) (4). The consensus ARE sequence has been extensively characterized (5).

The consensus binding sequence of erythroid transcription factor NF-E2 shows high similarity to the ARE/EpRE sequence. Also, the expression profile of Nrf2, one of the NF-E2 subunit factors, overlaps with those of drug-metabolizing enzymes such as GST and NQO1. Based on these facts, we recently demonstrated that transcription factor Nrf2 (6–8) is essential for the coordinated transcriptional activation of genes encoding the drug-metabolizing enzymes, such as GST and NQO1, via AREs/EpREs (9). Nrf2-deficient mice fed with butylated hydroxyanisole, which normally leads to a pronounced up-regulation of Alpha, Pi, and Mu classes of GSTs and NQO1, failed to induce either of these detoxication enzymes in the liver or intestine (9). Since these detoxication enzymes decrease the level of oxidative stress by removing compounds capable of generating ROS or other highly reactive substances, they thereby constitute part of the defense mechanism against oxidative stress (10). Because ARE-type *cis*-acting sequences are frequently found in the regulatory regions of a number of other oxidative stress-inducible genes (5, 11–13), we hypothesized that Nrf2 might also serve as the key transcription factor activating these genes.

A number of defense proteins and activities in murine peritoneal macrophages are markedly induced upon exposure to electrophilic agents or other oxidative stresses. These proteins include heme oxygenase-1 (HO-1) (14–16), peroxiredoxin MSP23 (17), the cystine membrane transporter (system x_c^-) (18) and 60-kDa stress protein A170 (19). HO-1 is prominently induced under various oxidative stress conditions in many different cell types (14). HO-1-deficient embryonic fibroblasts are hypersensitive to the cytotoxicity of both hemin and hydrogen peroxide (15). Induction of system x_c^- activity increases the intracellular cysteine pool, which consequently augments the synthesis of GSH (20), a potent antioxidant with a short half-life. MSP23 is the murine peroxiredoxin I with antioxidative activity (21). It was recently shown that a mammalian peroxiredoxin isoform reduces the intracellular hydrogen peroxide level utilizing thioredoxin as an immediate electron donor (22) and protects cells from apoptosis by oxidative stress (23). A170 has a structural domain that interacts with ubiquitin (24) and PKC-ζ (25). Electrophilic agents, such as diethylmaleate (DEM), and other oxidative stress agents have been reported to induce the proteins HO-1, A170, MSP23, and system x_c^- activity in peritoneal macrophages (20) and fibroblasts (26). To determine whether these antioxidant stress proteins are also under the regulation of Nrf2, we examined in this study the electrophilic induction of this group of genes in peritoneal macrophages from the *nrf2*-null mutant mouse.

* This work was supported in part by grants-in-aid from the Ministry of Education, Science, Sports and Culture, the Japanese Society for Promotion of Sciences (JSPS), and CREST. The costs of publication of this article were defrayed in part by the payment of page charges. This article must therefore be hereby marked "*advertisement*" in accordance with 18 U.S.C. Section 1734 solely to indicate this fact.

‡ These two authors contributed equally to this work.
§ Research Fellow of the JSPS.
¶ To whom correspondence should be addressed: Center for TARA, University of Tsukuba, 1-1-1 Tennoudai, Tsukuba 305-8577, Japan. Tel.: 81-298-53-6158; Fax: 81-298-53-7318; E-mail: masi@tara.tsukuba.ac.jp.

[1] The abbreviations used are: ROS, reactive oxygen species; GST, glutathione *S*-transferase; NQO1, NAD(P)H:quinone oxidoreductase; EpRE, electrophile-responsive element; ARE, antioxidant-responsive element; HO-1, heme oxygenase-1; DEM, diethylmaleate; MTT, 3-[4,5-dimethylthiazol-2-yl]-2,5-diphenyltetrazolium bromide; CDNB, 1-chloro-2,4-dinitrobenzene; *t*-BHQ, *t*-butylhydroquinone; LPS, lipopolysaccharide; EMSA, electrophoretic mobility shift assay; MARE, Maf recognition element; StRE, stress-responsive element.

EXPERIMENTAL PROCEDURES

Culture of Macrophages—Female wild type ICR and *nrf2* mutant mice (9) weighing 20–25 g received an intraperitoneal injection of 2 ml of 4% thioglycollate broth. Four days later, macrophages were collected by peritoneal lavage (17). The cells were resuspended at 7.5×10^5 cells/ml and cultured in RPMI 1640 medium containing 10% (v/v) fetal bovine serum as described previously (17). For the 3-[4, 5-dimethylthiazol-2-yl]-2,5-diphenyltetrazolium bromide (MTT) (27) assay, the cells were resuspended at 2×10^5 cells/ml and cultured in medium without fetal bovine serum. After 1 h of culture, stress agents were added to the medium. Final concentrations of the agents in the medium were 100 μM for DEM, paraquat, and hydrogen peroxide (H_2O_2); 80 μM for catechol; 20 milliunits/ml for glucose oxidase (GO); 5 μM for $CdCl_2$ and menadione (2-methyl-1,4-naphthoquinone); 10 μM for 1-chloro-2,4-dinitrobenzene (CDNB); 20 μM for iodoacetic acid; 2.5 μM for *t*-butylhydroquinone (*t*-BHQ) and sodium arsenite ($NaAsO_2$); and 1 ng/ml for lipopolysaccharide (LPS). The macrophages were harvested at the times indicated in the figure legends. Cell viability was measured by the MTT assay (27) and the trypan blue dye exclusion test.

RNA Blot Hybridization Analysis—Total cellular RNA was extracted from macrophages by RNAzol™ B (TEL-TEST, Inc., Friendswood, TX). The RNA samples (10 μg) were electrophoresed and transferred to Zeta-Probe GT membranes (Bio-Rad). The membranes were probed with ^{32}P-labeled cDNA probes as indicated in the figure legends. β-Actin cDNA was used as a positive control.

Immunoblotting—Macrophages were solubilized with SDS-sample buffer (without dye or 2-mercaptoethanol), and protein concentrations were estimated by the BCA protein assay (Pierce). The proteins were separated by SDS-polyacrylamide gel electrophoresis in the presence of 2-mercaptoethanol and electrotransferred onto Immobilon membrane (Millipore Corp., Bedford, MA). To detect immunoreactive proteins, we used horseradish peroxidase-conjugated anti-rabbit IgG and ECL blotting reagents (Amersham Pharmacia Biotech). Polyclonal rabbit antisera raised against rat HO-1, rat MSP23, and recombinant murine A170 were used as described previously (19, 21). Specific antibody was raised against Nrf2 by immunizing rabbits with recombinant Nrf2 protein (amino acids 140–318 fused with *E. coli* maltose-binding protein). An anti-actin antiserum was purchased from Santa Cruz Biotechnology, Inc. (Santa Cruz, CA). Densitometric analysis was performed using NIH Image software.

Determination of Cystine Uptake and GSH Level—Cystine transport activity was measured using ^{14}C-labeled cystine in phosphate-buffered saline containing 0.1% glucose as described previously (20). Total (*i.e.* reduced plus oxidized) GSH was extracted from macrophages with 5% trichloroacetic acid solution, and GSH content was measured as described previously (20).

Transient Transfection Assay—The quail fibroblast cell line QT6 (28) was maintained in Dulbecco's modified Eagle's medium supplemented with 10% fetal bovine serum and seeded in 24-well dishes 24 h before transfection. The cells were transfected with reporter (pHO-1-Luc (see "Results") and pRBGP2 (7)) plasmids and an effector plasmid (cNrf2; Ref. 7) using calcium phosphate precipitation as described previously (29). The Luciferase assay was performed by utilizing the Luciferase Assay System (Promega, Madison, WI) following the supplier's protocol and measured in a Biolumat Luminometer (Berthold, Germany). Transfection efficiencies were routinely normalized to the activity of a co-transfected β-galactosidase expression plasmid, pENL. Normally, three independent experiments, each carried out in duplicate, were performed, and the results were averaged. The cells were washed 12 h after transfection, and then DEM (Wako, Tokyo) was immediately added to the culture medium.

Electrophoretic Mobility Shift Assay (EMSA)—Nuclear extracts were prepared from macrophages as described previously (7). An oligonucleotide containing the stress-responsive element of the *ho-1* AB1 enhancer (5′-TCTGTTTTCGCTGAGTCATGGTTCCCGTTG-3′) was labeled with [γ-^{32}P]ATP by T4 polynucleotide kinase. EMSA was performed as described previously (7). Where indicated, antibodies were included in the binding reaction at 1:10 to 1:100 dilutions. The anti-chicken MafK antibody was described previously (9), and that against human Nrf2 was purchased from Santa Cruz Biotechnology. In competition experiments, a 100-fold excess of unlabeled double-stranded oligonucleotides was included in the reaction (7).

RESULTS

Impaired Induction of Antioxidative Stress Proteins in Nrf2-deficient Macrophages—A number of proteins or activities are induced by electrophilic agents in murine peritoneal macrophages. To test whether the electrophilic induction of this group of genes shares a common regulatory mechanism with that of the drug-metabolizing enzymes, we examined their expression in Nrf2-deficient macrophages. Peritoneal macrophages were harvested from *nrf2*-homozygous and -heterozygous mutant (or wild type) female ICR siblings. The macrophages were then independently challenged with DEM (an electrophilic agent), paraquat (an O_2^- generator), GO (an H_2O_2 generator), or $CdCl_2$ (heavy metal). After challenging macrophages with these agents, we examined expression levels of three oxidative stress-inducible proteins (below) by immunoblotting and RNA blotting analyses. Since wild type and heterozygous mutant mice did not show large differences in induction of the antioxidative proteins, we used both types of macrophages as positive controls.

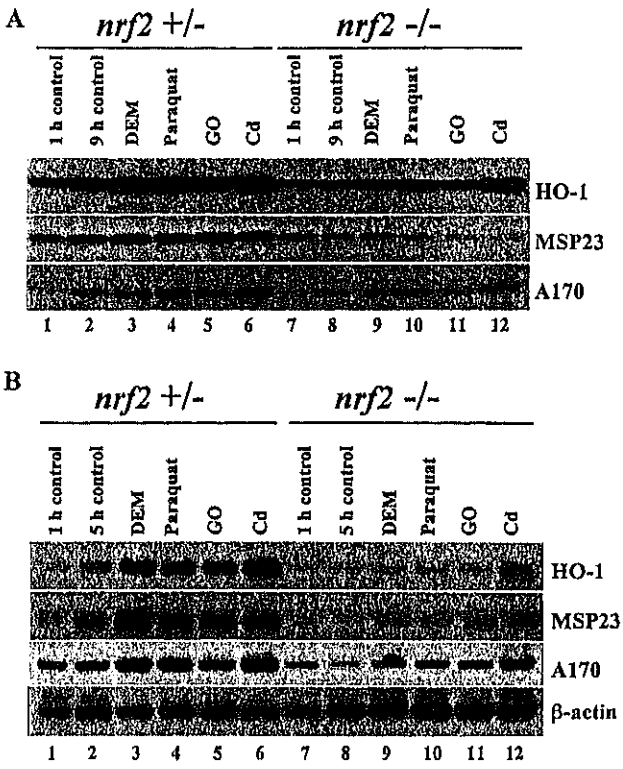

FIG. 1. **Stress agent-dependent loss of HO-1, MSP23, and A170 gene induction in Nrf2-deficient macrophages.** *A*, immunoblot analysis of the effects of oxidative stress agents on the expression levels of HO-1 (34 kDa), MSP23 (23 kDa), and A170 (60 kDa). Macrophages from *nrf2*-heterozygous (+/−) (*lanes 1–6*) and homozygous (−/−) (*lanes 7–12*) mutant mice were cultured for 1 h (*lanes 1* and *7*) or 9 h (*lanes 2* and *8*). Stress agents were added to the culture medium after a 1-h culture, and the macrophages were incubated with the agents for another 8 h (*lanes 3–6* and *9–12*). The stress agents added were DEM (*lanes 3* and *9*), paraquat (*lanes 4* and *10*), GO (*lanes 5* and *11*), and $CdCl_2$ (*lanes 6* and *12*). *B*, RNA blot analysis of the effects of oxidative stress agents on the levels of mRNAs for HO-1, MSP23, and A170. Total RNAs were prepared from macrophages cultured for 1 h (*lanes 1* and *7*) or 5 h (*other lanes*). Stress agents were added at 1 h after the start of the culture. *Lane* arrangements are as in *A*.

We first measured the levels of HO-1, MSP23, and A170 proteins 1 h after the start of *in vitro* culture and found that the basal levels of these proteins in the heterozygous macrophages were similar to those of *nrf2*-homozygous mutant macrophages (Fig. 1*A*, *lanes 1* and *7*). After transfer of the *nrf2*-heterozygous cells to *in vitro* culture, these stress-inducible proteins were gradually induced by unknown mechanisms (compare *lanes 1* and *2*). The gradual induction of HO-1 and MSP23 expression was not seen in Nrf2-deficient cells (*lanes 2* and *8*). The important finding here was that whereas all of the stress agents

TABLE I
Quantitative analysis of the induction of HO-1 and MSP23 proteins by various stress agents

The protein levels were calculated from densitometrical analysis of the immunoblot bands. Results are mean ± S.D. of 3–5 separate experiments. The standard levels (1.00) are those of cells cultured for 9 h without agents. The culture conditions are the same as in Fig. 1A.

Agents	HO-1		MSP23	
	Nrf2 (+/−)	Nrf2 (−/−)	Nrf2 (+/−)	Nrf2 (−/−)
	relative absorbance			
None (1 h)	0.58 ± 0.02	0.50 ± 0.19	0.60 ± 0.17	0.50 ± 0.25
None (9 h)	1.00	0.57 ± 0.12	1.00	0.50 ± 0.16
DEM	1.67 ± 0.17	0.69 ± 0.04	1.83 ± 0.04	0.54 ± 0.30
CDNB	2.94 ± 0.21	0.77 ± 0.02	1.51 ± 0.69	0.34 ± 0.08
GO	1.22 ± 0.02	0.57 ± 0.07	1.51 ± 0.02	0.34 ± 0.21
H_2O_2	1.26 ± 0.10	0.55 ± 0.06	0.97 ± 0.27	0.38 ± 0.14
t-BHQ	1.91 ± 0.77	0.86 ± 0.47	1.58 ± 0.07	0.44 ± 0.27
Menadione	6.38 ± 3.93	4.54 ± 2.76	1.94 ± 0.10	0.58 ± 0.21
Catechol	3.70 ± 0.02	1.77 ± 0.06	1.75 ± 0.06	0.52 ± 0.17
$CdCl_2$	1.57 ± 0.14	1.21 ± 0.08	1.38 ± 0.22	0.35 ± 0.15
Paraquat	1.34 ± 0.03	0.88 ± 0.03	1.50 ± 0.28	0.55 ± 0.25
$NaAsO_2$	3.70 ± 1.30	1.08 ± 0.51	1.01 ± 0.11	0.43 ± 0.16
Iodoacetic acid	2.05 ± 0.10	0.98 ± 0.27	1.15 ± 0.17	0.60 ± 0.27

tested induced HO-1, MSP23, and A170 in *nrf2*-heterozygous cells, induction was largely canceled in Nrf2-deficient cells. Closer examination revealed that in *nrf2*-null mutant cells (*lanes 9–12*) induction of HO-1 and A170 by DEM and GO was severely affected, but induction by paraquat and $CdCl_2$ was less impaired. In contrast, while MSP23 was markedly induced by these agents in *nrf2*-heterozygous cells, induction was largely absent in *nrf2*-null mutant cells.

Quantitative Analysis of Antioxidative Stress Protein Induction by Various Stress Agents—We also examined induction of these proteins by other stress agents: catechol, CDNB, H_2O_2, iodoacetic acid, sodium arsenite, menadione, and *t*-BHQ. Quantitative analysis by densitometry of the stained bands is shown in Table I. Menadione and catechol induced HO-1 in the Nrf2-deficient cells at levels comparable with those in *nrf2*-heterozygous mutant cells, suggesting the involvement of signal-transducing pathway(s) other than the Nrf2 system. Apparently, induction of HO-1 by sodium arsenite, *t*-BHQ, CDNB, and iodoacetic acid is largely, if not exclusively, dependent on the presence of Nrf2. A significant increase of MSP23 by all stress agents except sodium arsenite, H_2O_2, and iodoacetic acid was also observed in the heterozygous mutant cells but not in homozygous mutant cells (Table I). These results thus indicate that inducible expression of MSP23 is regulated mainly through the ARE/Nrf2 system.

To assess the induction process at the level of transcription, RNA was extracted from macrophages that had been treated with various stress agents and analyzed by the RNA blot analysis. Treatment with stress agents significantly increased the levels of HO-1 and MSP23 mRNA in *nrf2*-heterozygous cells (Fig. 1*B*, *lanes 1–6*), but the induction was markedly impaired in *nrf2*-null mutant cells (*lanes 7–12*). In contrast, whereas the lack of the induction of A170 mRNA in *nrf2*-null mutant cells was evident when DEM was used as the stress agent, the induction was only partially affected in Nrf2-deficient cells when paraquat, GO, or $CdCl_2$ was used as an inducer. Marked induction of the genes was also observed in the *nrf2*-heterozygous cells treated with menadione, *t*-BHQ, catechol, or CDNB (data not shown). The induction of HO-1 mRNA by menadione and catechol was diminished in Nrf2-null mutant cells, while that by *t*-BHQ and CDNB was largely abolished. Induction of MSP23 mRNA by all of these agents was markedly impaired in *nrf2*-null mutant cells. The three oxidative stress-inducible genes we addressed here showed roughly comparable variation in the mRNA and protein levels in response to various stress

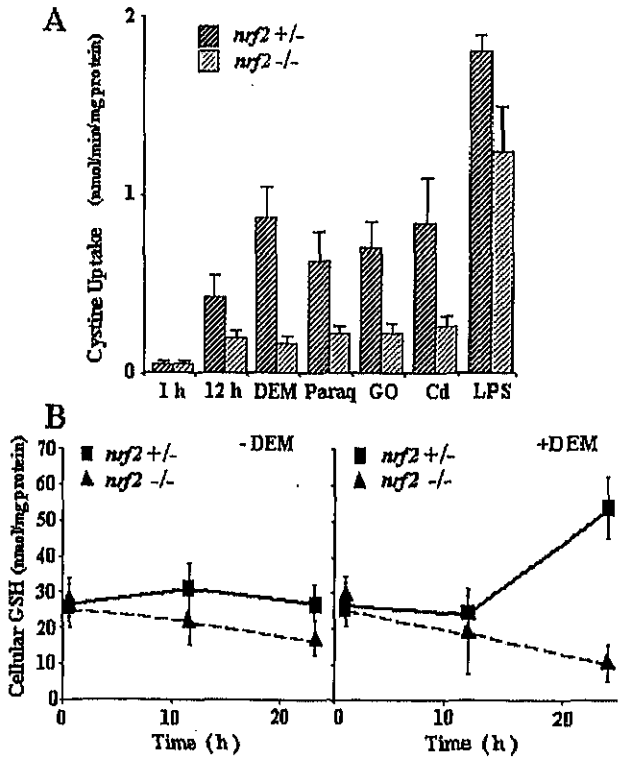

FIG. 2. **Oxidative stress agents do not induce system x_c^- or GSH in Nrf2-deficient macrophages.** *A*, inability to induce the system x_c^- cystine transport activity in the *nrf2*-deficient macrophages. Macrophages were incubated for 12 h with DEM, paraquat, GO, $CdCl_2$, and LPS as described in the legend to Fig. 1*A*. *B*, decreased cellular GSH level in *nrf2*-deficient macrophages treated with 100 μM DEM. The values in *A* and *B* represent mean ± S.E. of three independent experiments, each carried out in duplicate.

agents (Fig. 1, compare *A* and *B*, and data not shown). These results thus indicate that Nrf2 regulates the stress agent-mediated induction of HO-1, MSP23, and A170 gene expression. The results also clearly show that the contribution of Nrf2 to the transcriptional activation of these genes differed based upon the stress-inducing agent.

Induction of the Cystine Transporter x_c^- System Is Defective in Nrf2-deficient Cells—Because oxidative stress agents transcriptionally induce system x_c^- activity in macrophages (20, 26), the stress induction of system x_c^- activity in *nrf2*-null mutant cells was examined next (Fig. 2*A*). Whereas *nrf2*-heterozygous cells show system x_c^- activity comparable with that of wild type cells under both basal and induced conditions (data not shown), the oxidative stress agents DEM, paraquat, GO, and $CdCl_2$ barely induced system x_c^- activity in *nrf2*-null mutant cells (Fig. 2*A*). In contrast, LPS, a well known inducer of system x_c^- activity (30), significantly induced the system x_c^- activity even in *nrf2*-null mutant cells, indicating that LPS induction is mediated through an alternative regulatory pathway rather than the Nrf2 pathway. These results argue that the transcription of the cystine transporter gene may be under the regulatory influence of Nrf2.

It should be noted that system x_c^- activity is necessary to maintain a high GSH level in cultured macrophages, since cysteine is easily oxidized to cystine upon exposure to air (18). While the addition of 500 μM to 1 mM of DEM to the culture medium depletes the intracellular stores of GSH significantly, the addition of 100 μM DEM only diminishes the GSH level minimally, and then its level increases as a result of induced system x_c^- activity (26). As expected, the defect in inducible

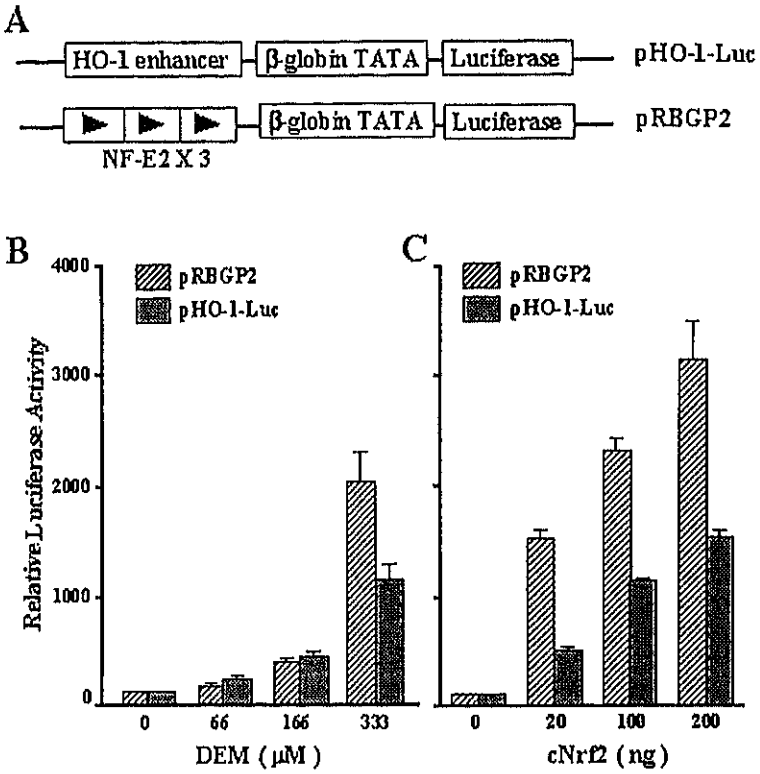

FIG. 3. **Overexpression of Nrf2 is sufficient to activate reporter gene expression driven by the AB1 enhancer of the *ho-1* gene.** *A*, schematic representation of the luciferase reporter constructs. In the HO-1-Luc reporter construct, a 161-base pair fragment of the AB1 enhancer of the *ho-1* gene is placed upstream of the rabbit β-globin TATA box and luciferase reporter gene. The pRBGP2 construct is similar, but three copies of the NF-E2 binding sequence from the chicken β-globin enhancer precede the TATA box and luciferase gene (7). *B*, pRBGP2 or pHO-1-Luc reporter construct was transfected into QT6 fibroblasts in the presence or absence of the electrophilic agent DEM. Luciferase activity in the absence of DEM was set at 100%, and results of three independent experiments each carried out in duplicate are shown with S.E. *C*, an increasing amount of chicken Nrf2 was transfected with pRBGP2 or pHO-1-Luc. Experiments were performed as in *B*.

expression of system x_c^- activity in *nrf2*-null mutant cells resulted in a decrease in cellular GSH content; after a 24-h incubation with DEM, the GSH level dropped to less than half its original level (Fig. 2*B*).

Overexpression of Nrf2 Up-regulates the Activities of the Distal Enhancer of the ho-1 Gene—The AB1 and SX2 enhancers of the *ho-1* gene (31) contain three and two copies, respectively, of the Maf recognition element (MARE), which largely overlaps with ARE (32). Due to their responsiveness to a wide variety of stress agents including oxidative stress, the MAREs were also named stress-responsive elements (StREs) (31–34). To ask whether Nrf2 can regulate the expression of this antioxidative stress gene via the *ho-1* AB1 enhancer, we co-transfected a Nrf2 expression plasmid and a *ho-1* AB1 enhancer-luciferase (pHO-1-Luc) reporter or β-globin enhancer-luciferase (pRBGP2) reporter into QT6 fibroblasts (Fig. 3*A*). DEM (Fig. 3*B*) and Nrf2 overexpression (Fig. 3*C*) both activated HO-1-Luc reporter gene expression, with the highest concentrations of these agents generating more than 10-fold activation. This increase was strictly dependent on the presence of the AB1 enhancer (data not shown). We also tested a pRBGP2 reporter that contains three tandem copies of the NF-E2 binding sequence of the chicken β-globin enhancer (7), a sequence that is very similar to the AB1 enhancer sequence. Interestingly, the pRBGP2 reporter responded more efficiently than the pHO-1-Luc reporter did to both DEM and the overexpression of Nrf2 (Fig. 3, *B* and *C*). These results indicate that StREs in the AB1 enhancer are actually responsible for the activation of *ho-1* gene expression and that Nrf2 can activate the *ho-1* gene expression through StREs.

Stress Agents Post-transcriptionally Induce DNA Binding Activity of Nrf2—Given the clear lack of inductive response in a number of electrophile-inducible genes, it was of interest to determine how oxidative stress agents activate Nrf2 and thereby induce a group of genes to counteract oxidative stress. To this end, we first examined the level of Nrf2 mRNA in macrophages under various oxidative stresses and found that the mRNA level was not changed significantly by any of the oxidative stress agents tested (Fig. 4*A*). In contrast, we found that these same stress agents significantly enhanced the DNA binding activity of Nrf2 to the StRE of HO-1 AB1 enhancer.

StRE binding activity in nuclear extracts was strongly induced by DEM treatment of macrophages, as revealed by the retarded band (*arrow* in Fig. 4*B*, *lanes 1* and *2*). The induction of binding activity was not observed in nuclear extracts prepared from *nrf2*-deficient cells (Fig. 4*B*, *lanes 3* and *4*). The complex was effectively competed by the addition of an excess of unlabeled StRE, mouse GST Ya gene ARE, or chicken β-globin enhancer NF-E2 binding site but not by a yeast Gal4 binding consensus sequence (Fig. 4*D*). This DNA-protein complex was markedly diminished by treatment with antibodies against mouse Nrf2 (Fig. 4*C*, *lane 3*) and chicken MafK (*lane 4*), which are partner molecules together comprising the heterodimeric transcription factor complex (34), but the decrease was not obvious using a normal rabbit IgG (*lane 5*). These results indicate that the DNA-protein complex contains both Nrf2 and small Maf proteins. The same binding activity was also induced in nuclear extracts of macrophages treated with GO, paraquat, or $CdCl_2$ (Fig. 4*E*). The Nrf2 expression level was also examined by immunoblotting analyses of nuclear extracts prepared from the macrophages treated with these stress agents. We found that DEM, GO, paraquat, $CdCl_2$, and CDNB all increased the Nrf2 level 1.5–3-fold (Fig. 4*F*). We therefore concluded that post-transcriptional regulation might be involved in the activation of Nrf2 by electrophilic agents and ROS.

Lack of Nrf2 Renders Macrophages Sensitive to Oxidative Stress—The analysis thus far clearly indicates that macrophages invoke an electrophile-inducible response upon exposure to oxidative stress agents and that the response is mediated by Nrf2. To ask whether this response has a major impact on cell viability, we incubated both *nrf2*-null and heterozygous control macrophages with 5–20 μM CDNB for 12 h and measured cell viability by the colorimetric MTT assay. While cell

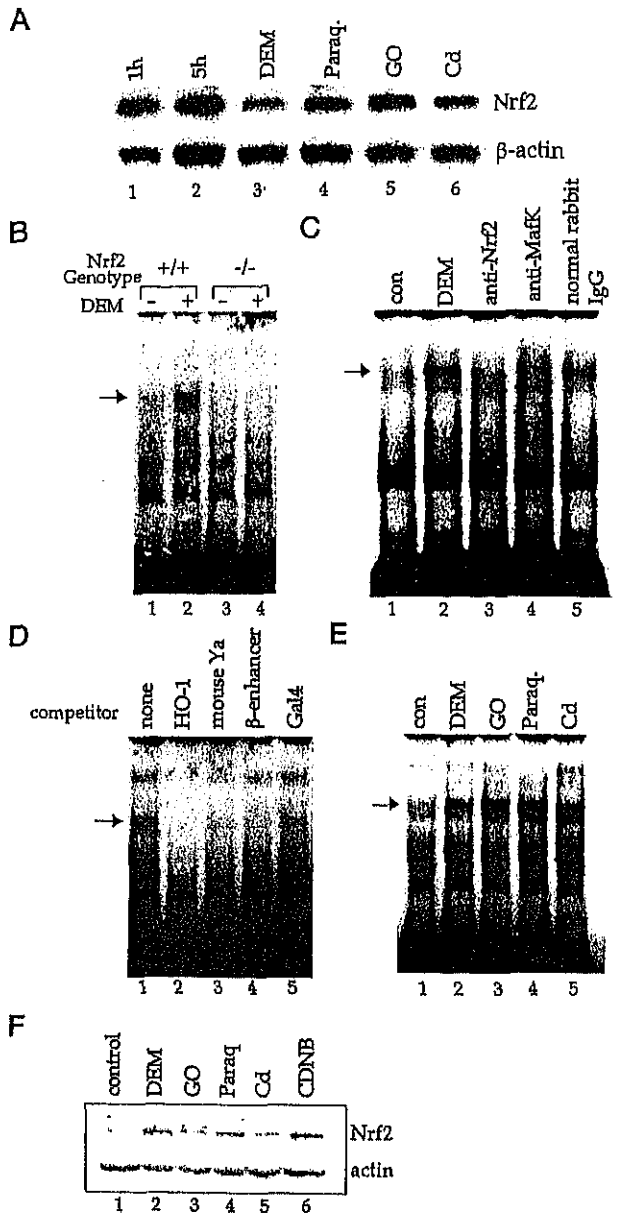

FIG. 4. **Increase in DNA binding activity of Nrf2-small Maf heterodimers upon exposure to stress agents.** *A*, RNA blot analysis of Nrf2 mRNA in macrophages treated with various stress agents. The *nrf2*-heterozygous mutant cells were incubated for 4 h with the stress agents as in Fig. 1*B*. Total RNAs extracted from the macrophages were analyzed with Nrf2 and β-actin cDNA probes. *B*, EMSA analysis of Nrf2-small Maf DNA binding activity in macrophage nuclear extracts. Nuclear extracts were prepared from wild type (*lanes 1* and *2*) or *nrf2*-deficient peritoneal macrophages (*lanes 3* and *4*). These macrophages were either treated with DEM for 4 h (*lanes 2* and *4*) or not treated (*lanes 1* and *3*). A double-stranded oligonucleotide of the StRE sequence in the *ho-1* gene AB1 enhancer (*ho-1* probe) was used as a probe. The complex containing Nrf2 is indicated by an *arrow*. *C*, Nrf2-small Maf heterodimer binds to StRE. The *ho-1* probe was incubated with the nuclear extract from control macrophages (*lane 1*) or the nuclear extract of macrophages treated with DEM (*lane 2*). Anti-Nrf2 (*lane 3*), anti-MafK (*lane 4*), or normal rabbit IgG (*lane 5*) was included in the reaction. The complex containing Nrf2 is indicated by an *arrow*. *D*, the binding specificity of the Nrf2-small Maf heterodimer was confirmed by an EMSA competition experiment. The *ho-1* probe was incubated with the nuclear extract of macrophages treated with DEM (*lane 1*). An excess of unlabeled probe oligonucleotide (*lane 2*) or double-stranded oligonucleotides from mouse GST Ya gene ARE (*lane 3*), chicken β-globin enhancer NF-E2 binding site (*lane 4*), or yeast transcription factor Gal4 cognate site (*lane 5*) was included in the binding reaction. The complex containing Nrf2 is indicated by an *arrow*. *E*, increase in the DNA binding activity of Nrf2-small Maf in stress agent-treated macrophages. Nuclear extracts were prepared from the peritoneal macrophages treated with DEM (*lane 2*), GO (*lane 3*), paraquat (*lane 4*), or $CdCl_2$ (*lane 5*) and examined by EMSA. An *arrow* indicates the complex containing Nrf2. *F*, increase of Nrf2 protein in the nucleus of the stress agent-treated macrophages. Immunoblotting analysis was performed with macrophage nuclear extracts.

TABLE II

CDNB sensitivity of Nrf2-null mutant macrophages

Both *nrf2*-heterozygous (+/−) and -homozygous (−/−) mutant macrophages were incubated with 0, 5, 10, and 20 μM CDNB for 12 h. The cell viability was examined with an MTT assay. Values are mean ± S.E. of relative absorbance of three independent experiments each carried out in duplicate. Both heterozygous and homozygous mutant cells showed similar absorbance in the MTT assay without CDNB. * $p < 0.05$.

CDNB	Sensitivity	
	Nrf2 (+/−)	Nrf2 (−/−)
μM	*relative absorbance*	
0	1.00	1.00
5	0.85 ± 0.09	0.86 ± 0.15
10	0.74 ± 0.06*	0.46 ± 0.13*
20	0.19 ± 0.02	0.22 ± 0.05

viability was decreased in both *nrf2*-null mutant and control macrophages treated with 20 μM CDNB, with 10 μM CDNB, *nrf2*-null mutant cells were more sensitive to the CDNB treatment than the heterozygous control cells (Table II). Notably, 10 μM CDNB treatment resulted in an approximately 2-fold difference in the MTT assay, and this difference is statistically significant ($p < 0.05$). The difference in the sensitivity to CDNB between the *nrf2*-null and -heterozygous cells was much clear when we measured the cell viability by the trypan blue dye exclusion test after 12 h of the CDNB treatment. The viability of the cells was 77 and 16% (mean of two independent experiments) for *nrf2*-heterozygous and *nrf2*-null mutant cells, respectively. Nrf2 thus appears to contribute significantly to cellular defense mechanisms against toxic electrophiles.

To highlight the Nrf2 contribution to cellular defense mechanisms, we pretreated macrophages for 36 h with 100 μM DEM, a concentration that potently induces the antioxidative stress response but with low cytotoxicity. The macrophages were subsequently treated with 5 or 10 μM CDNB for an additional 12 h. After incubation, we measured cell viability by trypan blue dye exclusion. The Nrf2-deficient macrophages were more sensitive to treatment with CDNB than the heterozygous control cells. After CDNB treatment, less than 20% of the Nrf2-deficient macrophages were viable (Fig. 5*B*), whereas more than 95% of the heterozygous cells were viable (Fig. 5*A*). These results unequivocally demonstrate that there are electrophile-inducible responses mediated by ARE/EpRE and Nrf2 and that the response machinery protects cells against toxic electrophiles and ROS stresses.

DISCUSSION

We demonstrate in this study that, in addition to the drug metabolizing enzymes that have already been shown to be regulated by the Nrf2 pathway (9), a group of oxidative stress-inducible genes is also under the immediate transcriptional influence of Nrf2-small Maf heterodimer regulatory proteins. The fact that Nrf2 regulates a group of stress-inducible protein genes via ARE/EpRE, as schematically illustrated in Fig. 6, is intriguing in the context of the physiological origin of these defense mechanisms. In an evolutionary sense, the acquisition of the ARE regulatory mechanism by genes that protect against oxidative stress seems to confer a significant advantage on the survival of living creatures. It should also be noted that,

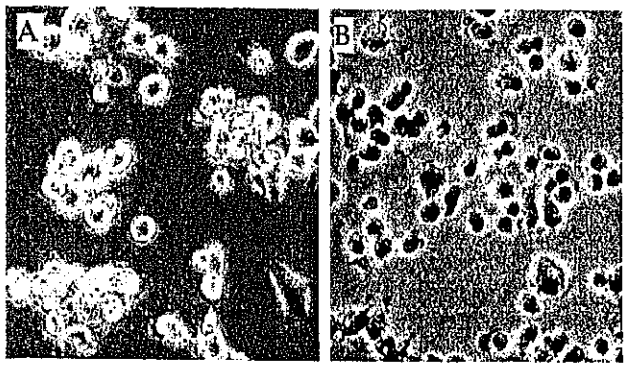

FIG. 5. **Nrf2-null mutant macrophages are sensitive to stress agents.** Both *nrf2*-heterozygous (+/−) (*A*) and homozygous (−/−) (*B*) mutant macrophages were first incubated with DEM for 36 h. After changing the medium, the cells were incubated with 10 μM CDNB for 12 h. Cell viability was examined with the trypan blue dye exclusion test.

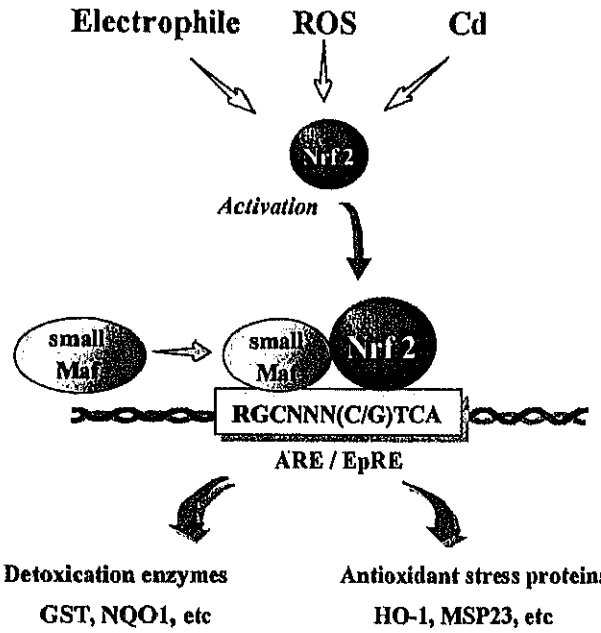

FIG. 6. **Schematic presentation of the antioxidative stress response through Nrf2 and ARE/EpRE.** The oxidative stress agents liberate Nrf2 from the cytoskeleton into the nucleus (40). Nrf2 then forms a heterodimer with a small Maf protein, interacts with ARE, and induces transcription of a set of genes that encode antioxidant functions. Nrf2 is a general regulator of the defense genes against oxidative stress, which include HO-1, MSP23, and system x_c^-, and also of a group of detoxication enzyme genes including GSTs and NQO1 (9).

whereas AREs are acquired by different categories of enzymes (*i.e.* detoxication enzymes and antioxidant proteins) during evolution, the transcription factors regulating the gene expression of these two categories have remained the same. Thus, an array of electrophile-responsive genes can be induced to act cooperatively upon exposure to toxic xenobiotics.

Three levels of regulation should be important for ARE/EpRE-mediated regulation of gene expression. First, the ARE/EpRE cognate sequence shares a high degree of similarity to the consensus MARE sequence (32, 35), so that AREs are competitively bound by a number of bZip transcription factors in the Maf, Jun, Fos, and Cap'n'Collar families. Second, heterodimer formation between these bZip factors creates another level of diversity of regulation (for a review, see Ref. 32). Third, transactivation through an ARE may be regulated coordinately during oxidative stress conditions. For example, the DNA binding activity of transcription factor AP-1 was inhibited when AP-1 was exposed to oxidative stress *in vitro* (36). This inhibition of AP-1 binding activity may allow the binding of other activating transcription factors, such as an Nrf2-small Maf heterodimer, to ARE and hence induce genes with protective properties against oxidative stress. An interesting extension of this speculation on the physiological roles of the bZip transcription factor network and its perturbation is that the oncogenic property of the bZip (*i.e.* Maf, Jun, and Fos family) factors may be in part due to the lack of a proper response to electrophiles or ROS, leaving the cells in a rather prooxidative state.

The AB1 and SX2 enhancers of the *ho-1* gene mediate the inducible expression of HO-1 by various stimuli (31, 33, 34). Multiple StREs reside in both *ho-1* enhancers and have been shown to play important roles in the regulation of *ho-1* gene expression by various electrophiles, ROS, heavy metals, and LPS (31, 33, 34). The StRE consensus sequence shares a high degree of similarity to those of ARE/EpRE and MARE (for a review, see Ref. 32), suggesting that StRE is also competitively bound by various bZip transcription factors. In this regard, we previously showed through gene targeting analysis that Nrf2 plays a central role in the regulation of GST and NQO1 gene expression through ARE (9), and the present study has extended the finding. We found that the inducible expression of the *ho-1* gene by electrophiles and ROS was severely affected in the Nrf2-null mutant macrophages. We also showed that Nrf2 could activate transcription of the reporter gene through the AB1 enhancer of the *ho-1* gene in a transfection assay. These results thus demonstrate that Nrf2 is one of the essential regulators of antioxidative stress genes acting through ARE/EpRE and StRE.

It should also be noted that Nrf2-dependence of stress-inducible gene expression appeared to differ from gene to gene. For instance, none of the electrophilic agents tested induced the expression of MSP23 in the *nrf2*-null mutant macrophages, whereas three of the agents, menadione, $CdCl_2$, and catechol, induced *ho-1* gene expression to a substantial level even in the *nrf2*-null mutant macrophages. We envisage that this variation in Nrf2 dependence reflects differences in the structures of the enhancers that mediate the stress signals to gene expression, since integration of signals from several stress-sensing pathways should be executed at the level of enhancer sequence. Indeed, accumulating evidence suggests that in addition to Nrf2, transcription factors NF-κB, AP-1, and heat shock factor are also activated in response to various oxidative stresses. Three lines of evidence further support this hypothesis. First, CAAT boxes, metal-responsive elements and NF-κB binding sequences are found in the *ho-1* enhancers (33, 37). Second, menadione is known to effectively activate NF-κB, perhaps by generating ROS (38). Third, NF-κB is also known to mediate signals from LPS (39). Based on these lines of evidence, we speculate that menadione most likely utilized the NF-κB pathway for *ho-1* gene induction in *nrf2*-null mutant cells. LPS induction of system x_c^- activity in Nrf2-null mutant cells might also be mediated by the NF-κB pathway.

Our present and previous studies uncovered the importance of Nrf2 in cellular protection against oxidative stress. This thesis was supported by the fact that induction of antioxidative stress genes by electrophilic agents was practically absent in the Nrf2-deficient macrophages. An important observation here is that the activation of Nrf2 by electrophilic agents and ROS did not accompany transcriptional induction of the *nrf2* gene (Fig. 4*A*). Based on this observation, we recently identified Keap1, a new factor that binds to the N-terminal Neh2 domain of Nrf2 and negatively regulates Nrf2 activity (40). Electrophilic agents liberate Nrf2 from Keap1 repression. The results

shown in Fig. 4 suggest a possibility that the stress agents facilitate translocation of Nrf2 from the cytosol to the nucleus. We are now investigating the precise molecular mechanism(s) whereby electrophilic agents and ROS affect interaction between the Neh2 domain of Nrf2 and Keap1.

Elevation of the cellular GSH level is one of the most important events in the electrophile-inducible defense response (2). The increase in GSH has been shown to be achieved by induction of a highly specific, sodium-independent, system x_c^- transport system for anionic cystine in exchange for glutamate. Interestingly, hepatic γ-glutamylcysteine synthetase, which catalyzes the rate-limiting step of *de novo* GSH synthesis, is also induced in mice fed on butylated hydroxyanisole (41) and in HepG2 cells treated with *t*-BHQ (42). Recently, multiple AREs in the distal enhancer of the γ-glutamylcysteine synthetase heavy subunit were reported to mediate inducible expression of the gene by β-naphthoflavone, an inducer of both phase I and II drug detoxifying enzymes (43). AREs in the murine ferritin L promoter (12) and metallothionein-I promoter (13) were also shown to be responsive to H_2O_2. Based on these broad observations, we speculate that many genes that function against oxidative stress are also regulated by Nrf2 via AREs. Thus, the Nrf2-centered gene expression regulatory system creates a coordinated cellular defense against a wide range of electrophilic compounds and ROS. Coordinated and inducible expression of these defense proteins should be important in preventing various free radical-related diseases, such as carcinogenesis, atherosclerosis, ischemia, and neurodegenerative disorders.

Acknowledgments—We thank Dr. Shigeru Taketani for providing polyclonal antibody against rat HO-1 and Drs. Kim-Chew Lim, Kazuhiko Umesono, Priscilla Wilkins Stevens, and Ruth T. Yu for productive discussions and assistance.

REFERENCES

1. Sies, H. (1991) *Am. J. Med.* **91**, Suppl. 3C, 31–38
2. Prestera, T., Zhang, Y., Spencer, S. R., Wilczak, C. A., and Talalay, P. (1993) *Adv. Enzyme. Regul.* **33**, 281–296
3. Friling, R. S., Bensimon, A., Tichauer, Y., and Daniel, V. (1990) *Proc. Natl. Acad. Sci. U. S. A.* **87**, 6258–6262
4. Rushmore, T. H., Morton, M. R., and Pickett, C. B. (1991) *J. Biol. Chem.* **266**, 11632–11639
5. Wasserman, W. W., and Fahl, W. E. (1997) *Proc. Natl. Acad. Sci. U. S. A.* **94**, 5361–5366
6. Moi, P., Chan, K., Asunis, I., Cao, A., and Kan, W. Y. (1994) *Proc. Natl. Acad. Sci. U. S. A.* **91**, 9926–9930
7. Itoh, K., Igarashi, K., Hayashi, N., Nishizawa, M., and Yamamoto, M. (1995) *Mol. Cell. Biol.* **15**, 4184–4193
8. Chui, D. H. K., Tang, W., and Orkin, S. H. (1995) *Biochem. Biophys. Res. Commun.* **209**, 40–46
9. Itoh, K., Chiba, T., Takahashi, S., Ishii, T., Igarashi, K., Katoh, Y., Oyake, T., Hayashi, N., Satoh, K., Hatayama, I., Yamamoto, M., and Nabeshima, Y. (1997) *Biochem. Biophys. Res. Commun.* **236**, 313–322
10. Prestera, T., and Talalay, P. (1995) *Proc. Natl. Acad. Sci. U. S. A.* **92**, 8965–8969
11. Inamdar, N. M., Ahn, Y. I., and Alam, J. (1996) *Biochem. Biophys. Res. Commun.* **221**, 570–576
12. Prestera, T., Talalay, P., Alam, J., Ahn, Y., Lee, P. J., and Choi, A. M. K. (1995) *Mol. Med.* **1**, 827–837
13. Dalton, T., Palmiter R. D., and Andrews, G. K. (1994) *Nucleic Acids Res.* **22**, 5016–5023
14. Keyse, S. M., and Tyrrell, R. M. (1989) *Proc. Natl. Acad. Sci. U. S. A.* **86**, 99–103
15. Poss, K. D., and Tonegawa, S. (1997) *Proc. Natl. Acad. Sci. U. S. A.* **94**, 10925–10930
16. Taketani, S., Sato, H., Yoshinaga, T., Tokunaga, R., Ishii, T., and Bannai, S. (1990) *J. Biochem. (Tokyo)* **108**, 28–32
17. Ishii, T., Yamada, M., Sato, H., Matsue, M., Taketani, S., Nakayama, K., Sugita, Y., and Bannai, S. (1993) *J. Biol. Chem.* **268**, 18633–18636
18. Bannai, S., and Tateishi, N. (1986) *J. Membr. Biol.* **89**, 1–8
19. Ishii, T., Yanagawa, T., Kawane, T., Yuki, K., Seita, J., Yoshida, H., and Bannai, S. (1996) *Biochem. Biophys. Res. Commun.* **226**, 456–460
20. Bannai, S., Sato, H., Ishii, T., and Taketani, S. (1991) *Biochim. Biophys. Acta* **1092**, 175–179
21. Ishii, T., Kawane, T., Taketani, S., and Bannai, S. (1995) *Biochem. Biophys. Res. Commun.* **216**, 970–975
22. Kang, S. W., Chae, H. Z., Seo, M. S., Kim, K., Baines, I. C., and Rhee, S. G. (1998) *J. Biol. Chem.* **273**, 6297–6302
23. Zhang, P., Liu, B., Kang, S. W., Seo, M. S., Rhee, S. G., and Obeid, L. M. (1997) *J. Biol. Chem.* **272**, 30615–30618
24. Vadlamudi, R. K., Joung, I., Strominger, J. L., and Shin, J. (1996) *J. Biol. Chem.* **271**, 20235–20237
25. Puls, A., Schmidt, S., Grawe, F., and Stabel, S. (1997) *Proc. Natl. Acad. Sci. U. S. A.* **94**, 6191–6196
26. Bannai, S. (1984) *J. Biol. Chem.* **259**, 2435–2440
27. Carmichael, J., DeGraff, W. G., Gazdar, A. F., Minna, J. D., and Mitchell, J. B. (1987) *Cancer Res.* **15**, 936–942
28. Moscovici, C., Moscovici, M. G., Jimenez, H., Lai, M. M., Hayman, M. J., and Vogt, P. K. (1977) *Cell* **11**, 95–103
29. Sambrook, J., Fritsch, E. F., and Maniatis, T. (1989) *Molecular Cloning: A Laboratory Manual*, 2nd Ed., Cold Spring Harbor Laboratory, Cold Spring Harbor, NY
30. Sato, H., Fujiwara, K., Sagara, J., and Bannai, S. (1995) *Biochem. J.* **310**, 547–551
31. Alam, J. (1994) *J. Biol. Chem.* **269**, 25049–25056
32. Motohashi, H., Shavit, J. A., Igarashi, K., Yamamoto, M., and Engel, J. D. (1997) *Nucleic Acids Res.* **25**, 2953–2959
33. Alam, J., Camhi, S., and Choi, A. M. K. (1995) *J. Biol. Chem.* **270**, 11977–11984
34. Choi, A. M. K., and Alam, J. (1996) *Am. J. Respir. Cell Mol. Biol.* **15**, 9–19
35. Kerppola, T. K., and Curran, T. (1994) *Oncogene* **9**, 3149–3158
36. Abate, C., Patel, L., Rauscher, F. J., and Curran, T. (1990) *Science* **249**, 1157–1161
37. Lavrovsky, Y., Schwartzman, M. L., Levere, R. D., Kappas, A., and Abraham, N. G. (1994) *Proc. Natl. Acad. Sci. U. S. A.* **91**, 5987–5991
38. Chen Q. I., and Cederbaum, A. I. (1997) *Mol. Pharmacol.* **52**, 648–657
39. Cordle, S. R., Donald, R., Read, M. A., and Hawiger, J. (1993) *J. Biol. Chem.* **268**, 11803–11810
40. Itoh, K., Wakabayashi, N., Katoh, Y., Ishii, T., Igarashi, K., Engel, J. D., and Yamamoto, M. (1999) *Genes Dev.* **13**, 76–78
41. Eaton, D. L., and Hamel, D. M. (1994) *Toxicol. Appl. Pharmacol.* **126**, 145–149
42. Galloway, D. C., Blake, D. G., Shepherd, A. G., and McLellan, L. I. (1997) *Biochem J.* **328**, 99–104
43. Moinova H. R., and Mulcahy, R. T. (1998) *J. Biol. Chem.* **273**, 14683–14689

Disruption of *nrf2* gene causes tooth decolorization: involvement of iron transport disorder

Toru Yanagawa[1], Ken Itoh[2], Akira Yamaguchi[4], Yasuaki Shibata[4], Tsuneyoshi Sano[5], Satoru Takahashi[2], Tetsuro Ishii[3], Hiroshi Yoshida[1], and Masayuki Yamamoto[2]

[1]Institute of Clinical Medicine, [2]Institute of Basic Medical Sciences and Center for Tsukuba Advanced Research Alliance, [3] Institute of Community Medicine, University of Tsukuba, 1-1-1 Tennodai, Tsukuba, 305-8575 Japan.

[4]Department of Oral Pathology, Nagasaki University School of Dentistry, 1-7-1 Sakamoto, Nagasaki, 852-8588, Japan

[5]Deaprtment of Oral Anatomy, Showa University School of dentistry, 1-5-8 Hatanodai, Shinagawa-ku, Tokyo 142-8585, Japan

Abstract

Background: Rodent teeth have a brownish color that reflects their iron content. During enamel maturation, iron is deposited onto the teeth surface by ameloblasts, in which iron is stored as ferritin containing-vesicles. Recently NF-E2-related factor 2 (*nrf2*)-deficient mice was created, which apparently develop normally, but closer examination revealed decolorization of the incisor.

Results: The teeth of the *nrf2*-deficient mice were grayish white, whereas those of wild-type mice are brownish yellow. Micro x-ray analysis revealed that the iron content on the tooth surface of *nrf2* knockout mice was significantly lower than that of wild-type mice. Immunohistochemical and *in situ* hybridization analysis showed that the expression level of ferritin mRNA in the *nrf2*-knockout mice was the same as that in wild-type in the early maturation stage. However, degenerative atrophy with iron deposition occurred in the ameloblast maturation stage in *nrf2*-deficient mice, and the ameloblasts disappeared in the early stage of tooth development. The acid resistance of the teeth was reduced in the *nrf2* deficient mice.

Conclusions: Our results suggest that the ameloblasts of *nrf2*-deficient mice have a defect in their iron transport systems, due to the lack of Nrf2, that resulted in disturbed iron excretion onto the enamel surface.

Introduction

The color of the teeth has been linked to their resistance to decay. Observant practitioners have noticed that individuals who are highly susceptible to dental caries have teeth of a grayish-white opacity (Bödcker, 1933). However, the relationship between caries resistance and tooth color has not been supported by statistical methods (Kerosuo& Kolehmainen, 1982).

It is well known that the brownish yellow color of the rodent incisor is owing to pigmentation that is largely derived from iron deposited on the enamel surface (Halse, 1973; Halse, 1974). In the rodent incisor, the layer of ameloblasts contains cells that represent the entire sequence of cell developmental stages. Secretory ameloblasts produce enamel matrix proteins and at the maturation stage the ameloblasts, in addition to their fundamental roles in enamel formation, incorporate iron and deposit it onto the surface layer of the mature enamel. In this unique iron transport system, ferritin functions as a transient iron reservoir in the cell, sequestering iron from the cytoplasm into these granules (Karim& Warshawsky, 1984).

Nrf2 belongs to the CNC family proteins, which share a conserved basic-leucine zipper domain first identified in the Drosophila cap'n'collar (CNC) protein (Mohler *et al.*, 1991). Nrf2 is essential for the transcriptional induction of phase II enzymes and antioxidant proteins via antioxidant responsive element (ARE)-mediated. Furthermore, Nrf2 constitutes a crucial cellular sensor for oxidative stress together with its cytoplasmic repressor Keap1, and mediates a key step in the signaling pathway by a novel Nrf2 nuclear

shuttling mechanism (Itoh *et al.*, 1999b). The activation of Nrf2 leads in turn to the induction of phase II enzyme and antioxidative stress genes in response to stresses (Ishii *et al.*, 2000; Itoh *et al.*, 1999a).

The creation of the *nrf2*-deficient mice was reported previously (Itoh *et al.*, 1997). Although this mutant line is very useful for the analysis of resistance to anti-cancer drugs and oxidative stress, no physiological phenotype has been described. We found that the maxillary incisor of the *nrf2*-deficient mice were decolorized, becoming grayish white. Here we have attempted to elucidate its mechanism in this study.

Results

Macroscopic observation

Mice homozygous for the *nrf2* mutation appear normal and fertile. Only the color of their incisors was different from that of the wild-type mice. Macroscopic observation revealed that the maxillary incisors of homozygous mutant (*nrf2*(-/-)) mice were always grayish white, but those of wild-type and heterozygous mutant (*nrf2*(+/-)) mice were brownish yellow, which is the normal color of rodent incisors (Fig. 1). We checked 50 offspring for the relationship between genotype and the incidence of decolorization by macroscopic observation. Of the mice with grayish-white incisors, all were homozygous for the *nrf2* mutation; the mice with brownish yellow incisors were all heterozygous or wild-type. Therefore, the penetration of decolorization phenotype was 100% ($p<0.001$ chi-square test).

Scanning electron microscopic observation

Scanning electron microscopic observation detected no structural differences in the surface of the teeth between wild-type and mutant mice (Fig. 2A, D), but X-ray microanalysis demonstrated an apparent change in the distribution and content of Fe on the enamel surfaces of the *nrf2*(-/-) mice. A dot-map image of the elements on the teeth surface showed remarkably decreased Fe distribution on the enamel surface of *nrf2*(-/-) teeth (Fig. 2F), compared with wild-type mice (Fig. 2C). The distribution pattern of Ca was not different between the wild-type (Fig. 2B) and (-/-) mice (Fig. 2E).

Table 1 summarizes the Ca, P, and Fe content of the incisors as quantified by X-ray

microanalysis. There was no significant differences in the mean weight % of Ca or P between the teeth of wild-type, *nrf2*(+/-) and *nrf2*(-/-) mice. The molar ratio of Ca to P was not different, either. In contrast, the mean weight % of the Fe of the *nrf2*(-/-) enamel was less than one-tenth that of wild-type mice. Between the wild-type and *nrf2* (+/-) mice there was also a significant difference in the Fe content. (i. e. that of *nrf2* (+/-) was about half of wild-type mice.

Immunohistochemistry, *in situ* hybridization, and iron staining

We used hematoxylin and eosin staining to compare the tooth development of *nrf2*(-/-) and wild-type mice (Fig. 3). In the rodent incisor, ameloblasts normally show their first sign of atrophy in the maturation stage. First their height is reduced, and finally they are changed to flat squamous cells on the incisal side. In our experiments, the ameloblasts in wild-type mice gradually shifted to become a cuboidal cell epithelium during the late maturation stage, whereas this change in *nrf2*(-/-) mice was rapid (Fig. 3A,B).

To understand the iron dynamics in the ameloblasts during enamel formation in wild-type and *nrf2*(-/-) mice, we investigated the localization of ferritin by immunohistochemical and *in situ* hybridization analysis. Iron localization was also detected using Berlin blue staining (Fig. 4). Iron, ferritin mRNA, and ferritin protein expression were observed to be the same in the ameloblasts during the transitional stage in both wild-type and *nrf2*(-/-) mice. Throughout the enamel-developing stage in wild-type mice, ferritin mRNA, ferritin and iron were located within the ameloblast cells (Fig. 4D-L). Ferritin was also observed in the papillary layer that supports the ameloblast cells (Fig. 4J-K). In wild-type mice, iron

was localized within the ameloblast cells (Fig. 4D, E). In the region of reduced ameloblasts in the wild-type mice, iron, ferritin mRNA, and ferritin protein disappeared gradually (Fig. 4F, I, L).

In the early maturation stage, ameloblast ferritin mRNA and protein localization was same for the *nrf2*(-/-) as for the wild-type mice, but the iron localization was different. In the *nrf2* (-/-) mice, iron was also located in the papillary layer. In the late maturation stage, the alignment of the papillary layer and the ameloblasts of the *nrf2*(-/-) mice first fell into disorder (Fig. 4N, Q, T, W), then the papillary layer disappeared. Finally, the junctions between the epithelial cells became loose, and the ameloblast layer became simple squamous epithelium (Fig. 4O, R, U, X). Although Berlin blue staining showed high levels of iron deposition in both the papillary layer and ameloblasts (Fig. 4P), as the ameloblasts degenerated during late maturation there was increased iron deposition in the papillary layer (Fig. 4Q). Following the degenerative atrophy, iron deposition was observed directly on the epithelium (Fig. 4R). At this stage the ferritin mRNA disappeared (Fig. 4U), but ferritin protein remained in the cells (Fig. 4X).

The acid resistance of teeth

To assess the quality of the *nrf2*(-/-) teeth, we investigated the acid resistance of *nrf2* (-/-) and wild-type tooth enamel. The enamel surface was exposed to 0.1 M acetate buffer at pH 4.0 and the amount of eluted calcium ion (Ca^{2+}) was determined. The rate of *nrf2*(-/-) tooth dissolution was faster than that of wild-type, and the concentration of eluted Ca^{2+} was significantly higher for *nrf2*(-/-) mice at 30 and 40 min ($P<0.05$: Student's t-test) (Fig. 5).

Thus the acid resistance of the teeth of the *nrf2*(-/-) mice was significantly lower than that of the wild-type mice.

Discussion

In this study we identified a phenotype of *nrf2*(-/-) mice and investigated why the incisors of *nrf2*(-/-) mice were grayish white. Our experiment revealed that this decolorization indicated the loss of iron. In the rodent incisor, the ameloblast layer contains cells from the entire sequence of developmental stages. In *nrf2*(-/-) mice, ameloblasts in the maturation stage showed degenerative changes and disappeared in the early stage of its developement. At the same time iron transport was disturbed, and the iron excretion onto the teeth surface was insufficient to maintain pigmentation in *nrf2*(-/-) mice.

Iron is critically involved in a wide variety of cellular events ranging from DNA synthesis to respiration. However, in the presence of physiological reducing agents, iron generates highly reactive oxygen species. Under these circumstances, iron is handled by transport and storage proteins. Within the cytosol, iron is incorporated into ferritin, in the form of inorganic ferric iron so that interaction with oxygen is minimal (Sies, 1997). Ferritin is expressed in ameloblasts at the early maturation stage (Miyazaki *et al.*, 1998) and is thought to be digested in the ferritin-containing vesicles that originate from lysosomes or other lytic bodies at the stage when the pigmentation of enamel begins (Kallenbach, 1970). Because Nrf2 was reported to bind to the ARE sequence upstream of the ferritin gene promoter (Beaumont *et al.*, 1994), we hypothesized that Nrf2 regulates the ferritin expression. However, our experiment shows that the expression level of ferritin does not

differ between *nrf2*(-/-) and wild-type ameloblasts by *in situ* hybridazation and immunohisitochemisitry, although the iron content does differ. The ferritin gene has many promoters and some other factor may be more important for its induction. In *nrf2*(-/-) mice, the defense system against oxidative stress does not function (Ishii *et al.*, 2000; Itoh *et al.*, 1999b). Because of this, the *nrf2*(-/-) ameloblast may become unable to protect itself from the excessive oxidative stress caused by iron, and may die from oxidative injury without depositing its iron on the enamel surface of the *nrf2*(-/-) teeth. Furthermore, we found that iron-poor *nrf2(-/-)* teeth lost acid resistance. This may indicate that rodents use the oxidative defense system not only to protect the cells from stress, but also to improve acid resistance of their teeth.

Here we demonstrated the mechanism underlying of the discoloration of teeth in the *nrf2*(-/-) mouse. However, the most proximal causative factor was not identified in this experiment, because *nrf2* regulates many kinds of genes, including a group of stress-inducible genes. We can hypothesize that heme oxygenase 1 is one of the candidates, among many stress-inducible proteins, because a mouse line lacking heme oxygenase 1 (Hmox1) was generated, and Hmox1 activity was shown to contribute predominantly to the extracelluar release of iron (Poss& Tonegawa, 1997a; Poss&Tonegawa, 1997b). Further study is necessary to identify the most influential factor in this iron transport disorder.

It has been thought that the color of teeth is associated with resistance to dental decay, and this hypothesis is partially supported by this experiment in rodent teeth. Because human teeth do not develop continuously like the rodent incisor does, events in the maturation stage of ameloblasts are transient during tooth development in humans.

However, this experiment showed an example of how a mutated gene could affect the dental resistance to acid in an animal that appears sound, even though it carries a genetic defect. This result indicates that dental color is a sign for morbidity for decay and for potential systemic unsoundness.

Experimental procedures

nrf2 deficient mouse

The *nrf2* mutant mice were developed at the Center for Tsukuba Advanced Research Alliance, University of Tsukuba as previously described (Itoh *et al.*, 1997). *nrf2* homozygous (*nrf2*(-/-)), *nrf2* heterozygous (*nrf2*(+/-)), and wild-type mice mice from multiple litters were used for this investigation. The incidence of phenotype was analyzed by the chi square test.

Scanning electron microscopic observation and micro x-ray analysis

The murine incisors, including the maxillary bone, were fixed in 100% ethanol and dehydraded by the critical point drying method. The incisors from *nrf2*(+/-) and *nrf2*(-/-) mice were examined using a scanning electron microscope (Hitachi S-2500CX) operated at 15 kV. Micro x-ray analysis was performed to determine the chemical components of the incisors. For energy-dispersive x-ray analysis, an x-ray detector system (Kevex Quantum Dealta IV) attached to a scanning electron microscope was used. The micro x-ray analysis system was operated at a 15-kV accelerating voltage and a 0.1-nA probe current, with a 20-

nm probe size, and a 100-sec counting time. Five points on the enamel surface were selected and analysis was carried out for the elements calcium (Ca), phosphorus (P), and iron (Fe).

In situ hybridazation, immunohistochemcal study, and iron staining

Ferritin-H cDNA was subcloned into the pBluescript KS^+ Vector and used as a template for cRNA production. DIG-11-UTP-labeled single-strand antisense and sense RNA probes were prepared with a DIG-RNA Labeling Kit (Boehringer Mannheim), using T7 or T3 RNA polymerase according to the manufacturer's instruction. Samples were fixed with 4% paraformaldehyde with PBS overnight at 4°C and decalcified in 10% EDTA (pH 7.4) for two weeks, embedded in paraffin, and sectioned. *In situ* hybridization was performed as described in (Shibata *et al.*, 2000). After treatment 0.2 N hydrochloric acid and Proteinase K (10 μg/ml), hybridization was performed with the probe (1 μg/ml) at 50° C overnight. After extensive washing and RNase A treatment, the hybridized DIG-labeled probes were detected with alkaline phosphatase-conjugated anti-DIG antibody and 5-bromo-4-chloro-3-indolyl phosphate as the substrate, using a nucleic acid detection kit (Boehringer Manheim). Controls included hybridization with the sense (mRNA) probe.

Immunostaining was performed using the labeled streptavidin biotin method (LsAB method: Nichirei). Sections were immersed in 0.3% hydrogen peroxide in methanol for 30 min, and incubated with 5% normal goat serum for 30 min at room temperature. The sections were then incubated with anti-ferritin rabbit polyclonal antibody (1:100 v/v) in PBS at 4°C overnight. The slides were reacted with biotinylated goat anti-rabbit or mouse

IgG antibody for 30 min at room temperature, followed by horseradish peroxidase conjugated with streptavidin. The peroxidase activity was visualized using the 3-amino-9-ethylcarbasol substrate-chromogen system (Nichirei, Tokyo), which resulted in red staining. The sections were counterstained with hematoxylin, dehydrated, and mounted. Control staining was performed with non-immune rabbit serum. Berlin blue staining was performed to detect iron ions.

Acid resistance

A 5 mm x 0.5 mm piece of the buccal surface of the murine incisors was exposed to 100 μl of 100 mM acetate buffer at pH 4.0 at room temperature. The eluted calcium ion was measured by the methylxylenol blue method (Calcium E test Wako, Wako) at 5, 10, 15, 20, 30, and 40 min. Standard deviations were based on five independent incisors from 8-12w wild-type or *nrf2*(-/-) mice.

Acknowledgements

This work was supported by Grants-in-Aid for Scientific Research and University of Tsukuba Research Projects. We thank Dr. Takanobu Isokawa for advice.

Table 1 Micro x-ray analysis of the incisors of *nrf2* mutant mice

The Ca, P, and Fe content of in the enamel surface of wild-type, (+/-), or (-/-) incisors as determined by micro x-ray analysis. The values represent the mean ± SD (n=5). Student's t-test was used for the statistical analysis.

Figure legends

Summary figure

We hypothesize that the ameloblasts of *nrf2*-deficient mice have an iron transport defect that leads to their degeneration and the failure to excrete iron onto the tooth surface.

Figure 1. Macroscopic view of the incisors from wild-type and *nrf2* homozygous mutant (*nrf2*(-/-)) mice.

The right panel shows the incisor of wild-type mice with the normal brownish-yellow color. The left panel shows the incisor of a *nrf2*(-/-) mice, which are always grayish white.

Figure 2. Electron microscopic observation with dot-map images.

Fig. 2 shows the scanning electron microscopic and dot-map images generated by micro x-ray analysis of the surface of the mouse incisor. (A) Incisors of a wild-type mouse; (D) Incisors of an *nrf2* homozygous mutant (*nrf2*(-/-)) mouse. (B and E) Dot-map images of calcium for both wild-type and *nrf2*(-/-) incisor surfaces. (C and F) Images of Fe on wild-type and *nrf2*(-/-) incisors, respectively. Although the dot-map image of the calcium content does not differ (Panel B, E), there is a remarkable difference between the iron images (Panel C, F). The raised iron concentration is shown on the surface of the teeth of a wild-type mouse (Panel C), while the iron concentration of the *nrf2*(-/-) teeth is very low, at the background level (F).

Figure 3. Immunohistochemistry and *in situ* hybridization

(A and B) Overview of wild-type and *nrf2* homozygous mutant (*nrf2*(-/-)) mouse incisor development (Panel A, wild-type; Panel B, *nrf2*(-/-)). The ameloblasts became degenerative and vanished earlier in the *nrf2*(-/-) mouse (40 x original magnification).

t: transition stage. em: early maturation stage. lm: late maturation stage. ra: region of reduced ameloblast.

Figure 4.

(A to X) Magnification of ameloblast on the enamel matrix at each stage. (A to L) Wild -type mouse. (M to X) *nrf2*(-/-) mouse. (A to C and M to O) Hematoxylin and eosin staining. (D to F and P to R) Berlin blue staining. (G to I and S to U) *In situ* hybridazation for ferritin. Positive signal is blue-purple. (J to L and V to X) Immunohistochemistry. Positive signal is red. The left column shows the early maturation stage; the middle column, late maturation stage; the right column, the region of reduced ameloblast. (100 x original magnification). pa: papillay layer, am: ameloblasts. arrow-head: iron deposition.

In the early maturation stage of wild-type mouse teeth (A, D, G J), iron and ferritin mRNA are located within the ameloblast cells. The ferritin protein is also located in the papillary layer by immunohistochemistry. In the early maturation stage of the *nrf2*(-/-) mouse (M, P, S, V), the location of ferritin mRNA and protein is same as wild-type, but iron is also located in the papillary layer (arrowheads), it is not in wild-type ameloblasts. During the late maturation stage and in the region of reduced ameloblast of the wild-type mouse,

the iron, ferritin mRNA, and ferritin protein disappear gradually and the ameloblasts's height is reduce (E, F, H, I, K, L). In the late maturation stage of the *nrf2*(-/-) mouse, the ameloblasts undergo degenerative atrophy, and iron deposition in the papillary layer increases (N). Finally, iron deposition accumulates on the atrophic ameloblasts (U).

Figure 5. Acid resistance of the enamel surface.

A 0.5 mm x 5 mm area on the buccal surface of murine incisors was exposed to acetate buffer at pH 4.0, and the amount of eluted calcium ion was determined. The surface of the *nrf2*(-/-) tooth eroded significantly earlier in acetic acid than did that of the wild-type mice. * $P<0.05$: Student's t-test.

References

Beaumont, C., Seyhan, A., Yachou, A.K., Grandchamp, B., Jones, R. (1994) Mouse ferritin H subunit gene. Functional analysis of the promoter and identification of an upstream regulatory element active in erythroid cells. *J Biol Chem* 269,20281-20288.

Bödecker, C.F. (1933) The color of the teeth as an index of their resistance to decay. *Int. Orthodont* **19**,386-392.

Halse, A. (1973) Effect of dietary iron deficiency on the pigmentation and iron content of rat incisor enamel. *Scand J Dent Res* **81**,319-334.

Halse, A. (1974) Electron microprobe analysis of iron content of incisor enamel in some species of Rodentia. *Arch Oral Biol* **19**,7-11.

Ishii, T., Itoh, K., Takahashi, S., et al. (2000) Transcription factor Nrf2 coordinately regulates a group of oxidative stress-inducible genes in macrophages. *J Biol Chem* **275**,16023-16029.

Itoh, K., Chiba, T., Takahashi, S., et al. (1997) An Nrf2/small Maf heterodimer mediates the induction of phase II detoxifying enzyme genes through antioxidant response elements. *Biochem Biophys Res Commun* **236**,313-322.

Itoh, K., Ishii, T., Wakabayashi, N., Yamamoto, M. (1999a) Regulatory mechanisms of cellular response to oxidative stress. *Free Radic Res* **31**,319-324.

Itoh, K., Wakabayashi, N., Katoh, Y., et al. (1999b) Keap1 represses nuclear activation of antioxidant responsive elements by Nrf2 through binding to the amino-terminal Neh2 domain. *Genes Dev* **13**,76-86.

Kallenbach, E. (1970) Fine structure of rat incisor enamel organ during late pigmentation and regression stages. *J Ultrastruct Res* **30**,38-63.

Karim, A., Warshawsky, H. (1984) A radioautographic study of the incorporation of iron 55 by the ameloblasts in the zone of maturation of rat incisors. *Am J Anat* **169**,327-335.

Kerosuo, E., Kolehmainen, L. (1982) The relationship between past caries experience and tooth color determined by an opto-electronic method. *Acta Odontol Scand* **40**,451-457.

Miyazaki, Y., Sakai, H., Shibata, Y., et al. (1998) Expression and localization of ferritin mRNA in ameloblasts of rat incisor. *Arch Oral Biol* **43**,367-378.

Mohler, J., Vani, K., Leung, S., Epstein, A. (1991) Segmentally restricted, cephalic expression of a leucine zipper gene during Drosophila embryogenesis. *Mech Dev* **34**,3-9.

Poss, K.D., Tonegawa, S. (1997a) Heme oxygenase 1 is required for mammalian iron reutilization. *Proc Natl Acad Sci U S A* **94**,10919-10924.

Poss, K.D., Tonegawa, S. (1997b) Reduced stress defense in heme oxygenase 1-deficient cells. *Proc Natl Acad Sci U S A* **94**,10925-10930.

Shibata, Y., Fujita, S., Takahashi, H., Yamaguchi, A., Koji, T. (2000) Assessment of decalcifying protocols for detection of specific RNA by non-radioactive in situ hybridization in calcified tissues. *Histochem Cell Biol* **113**,153-159.

Sies, H., editor (1997). Antioxidants in disease mechanisims and therapy. San diego: Academic press.

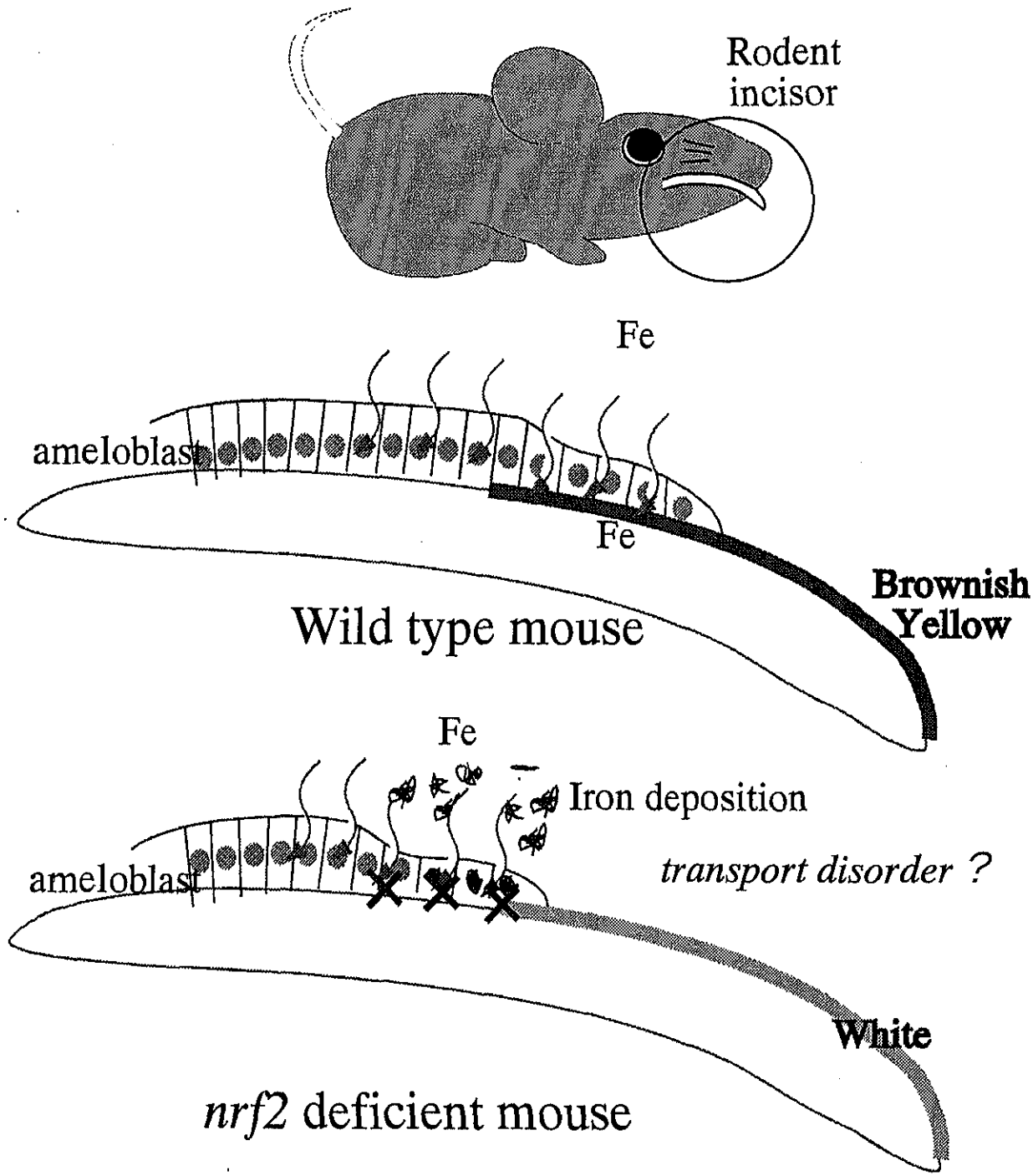

Summary figure

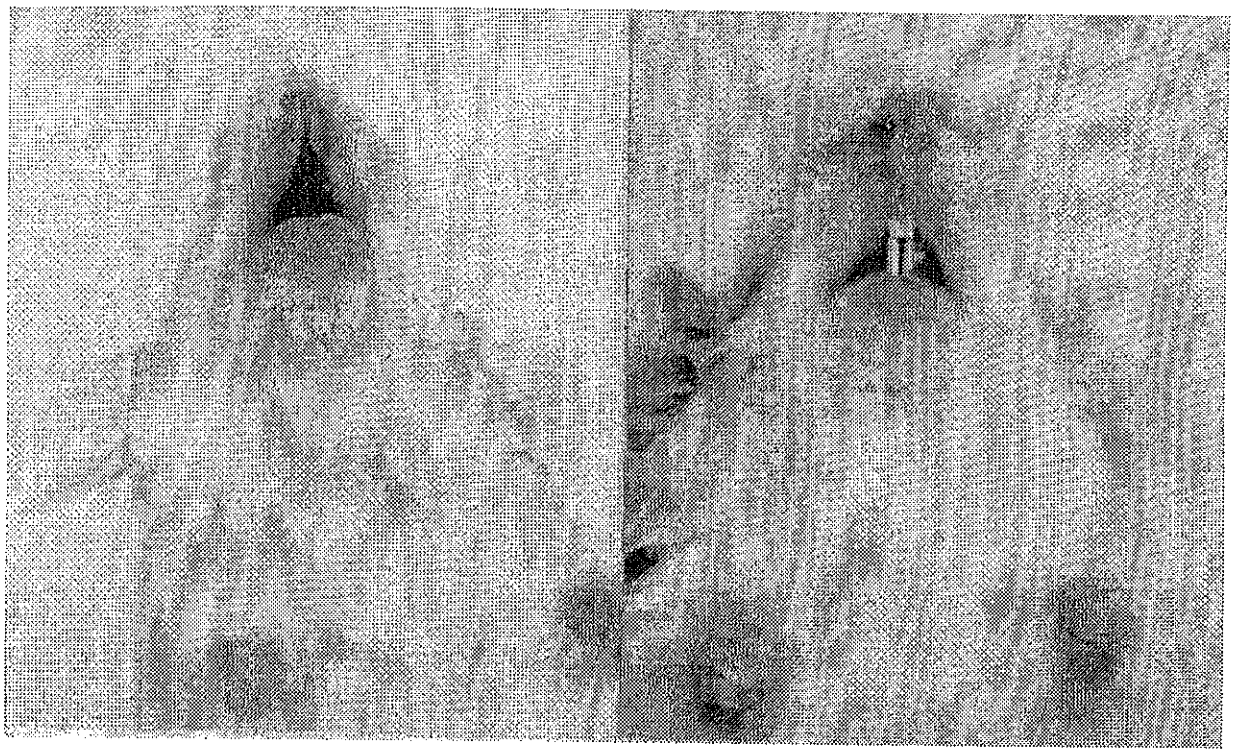

Fig.1

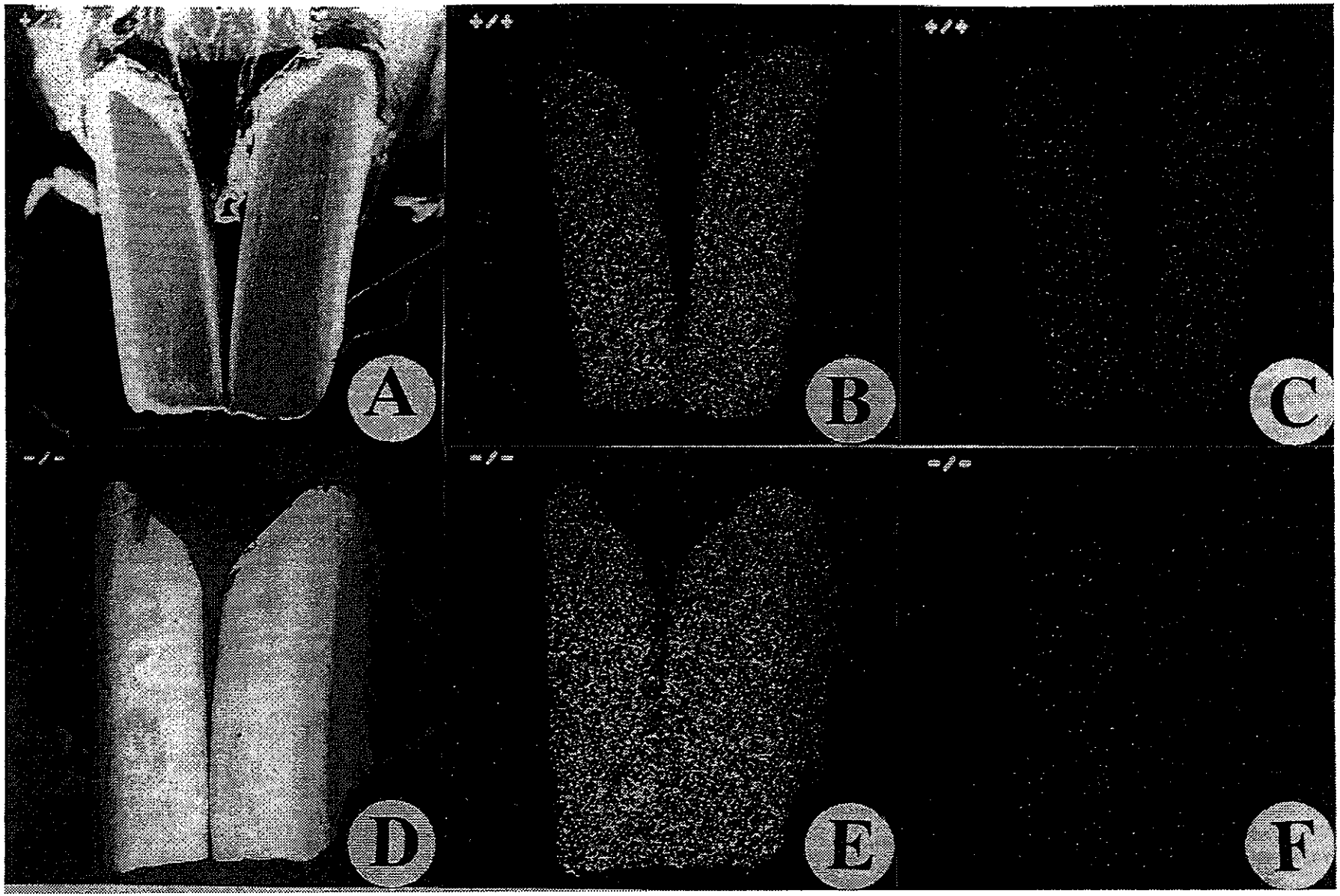

Fig.2

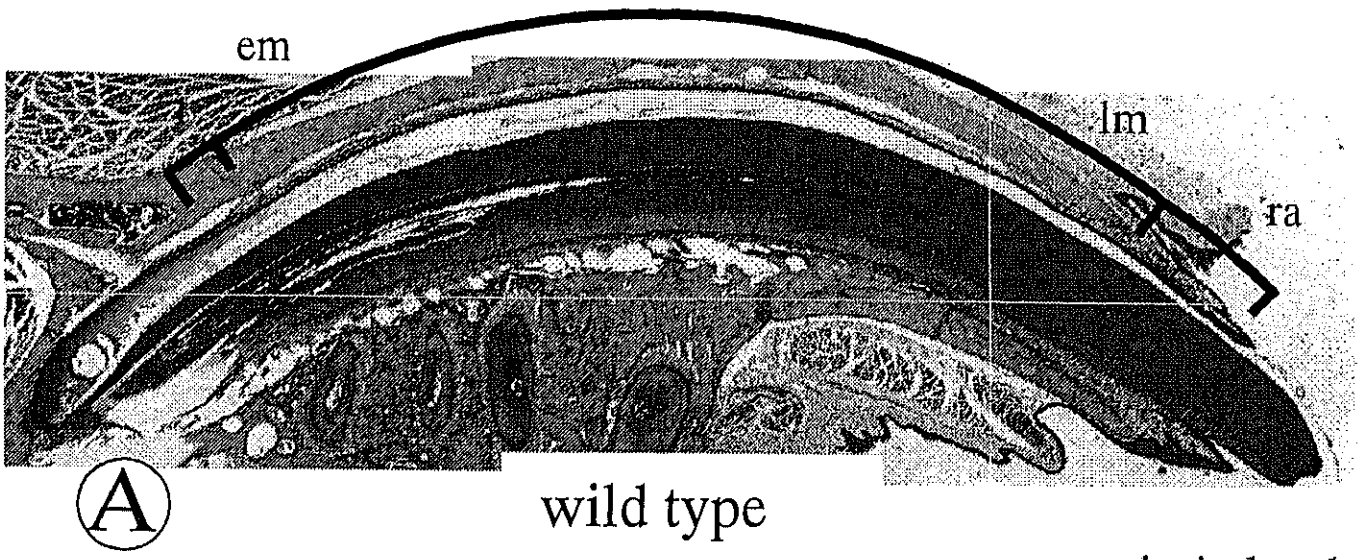
maturation stage
em
lm
ra
A
wild type
incisal end

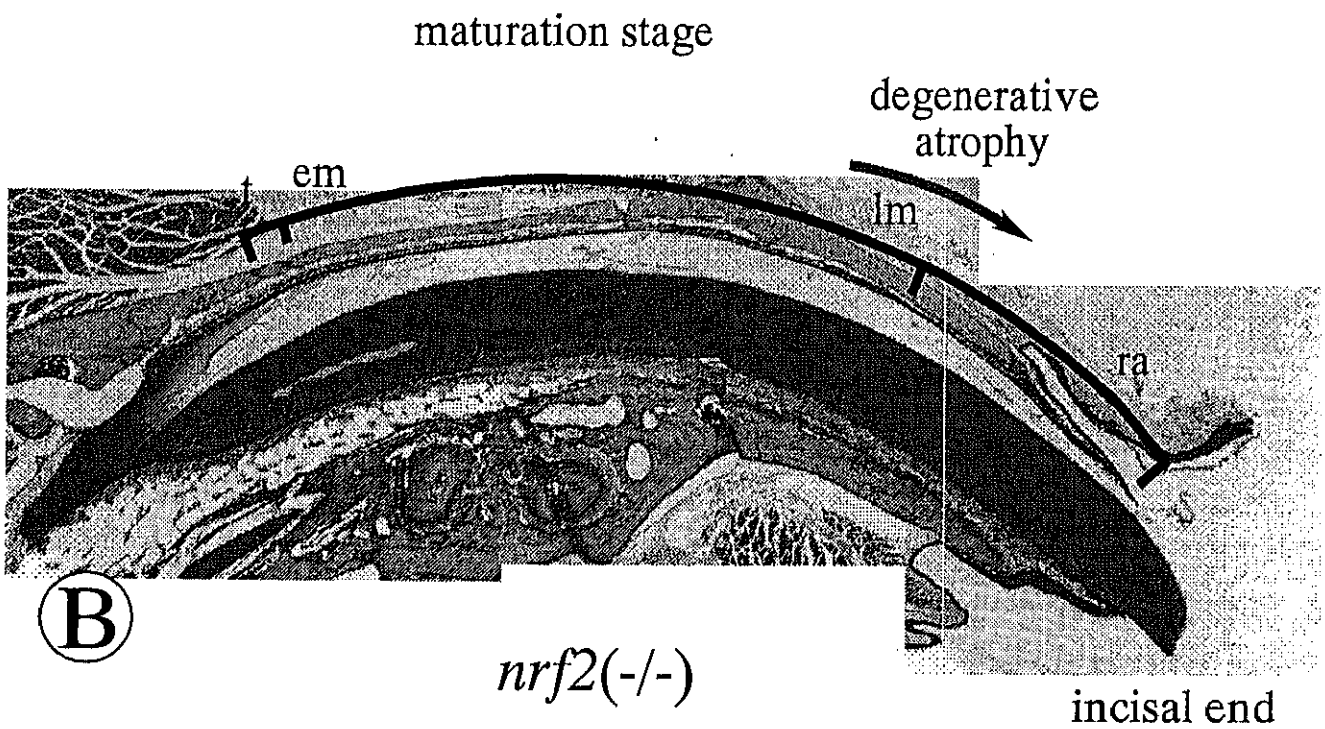
maturation stage
degenerative
atrophy
em
lm
ra
B
nrf2(-/-)
incisal end

Figure 3

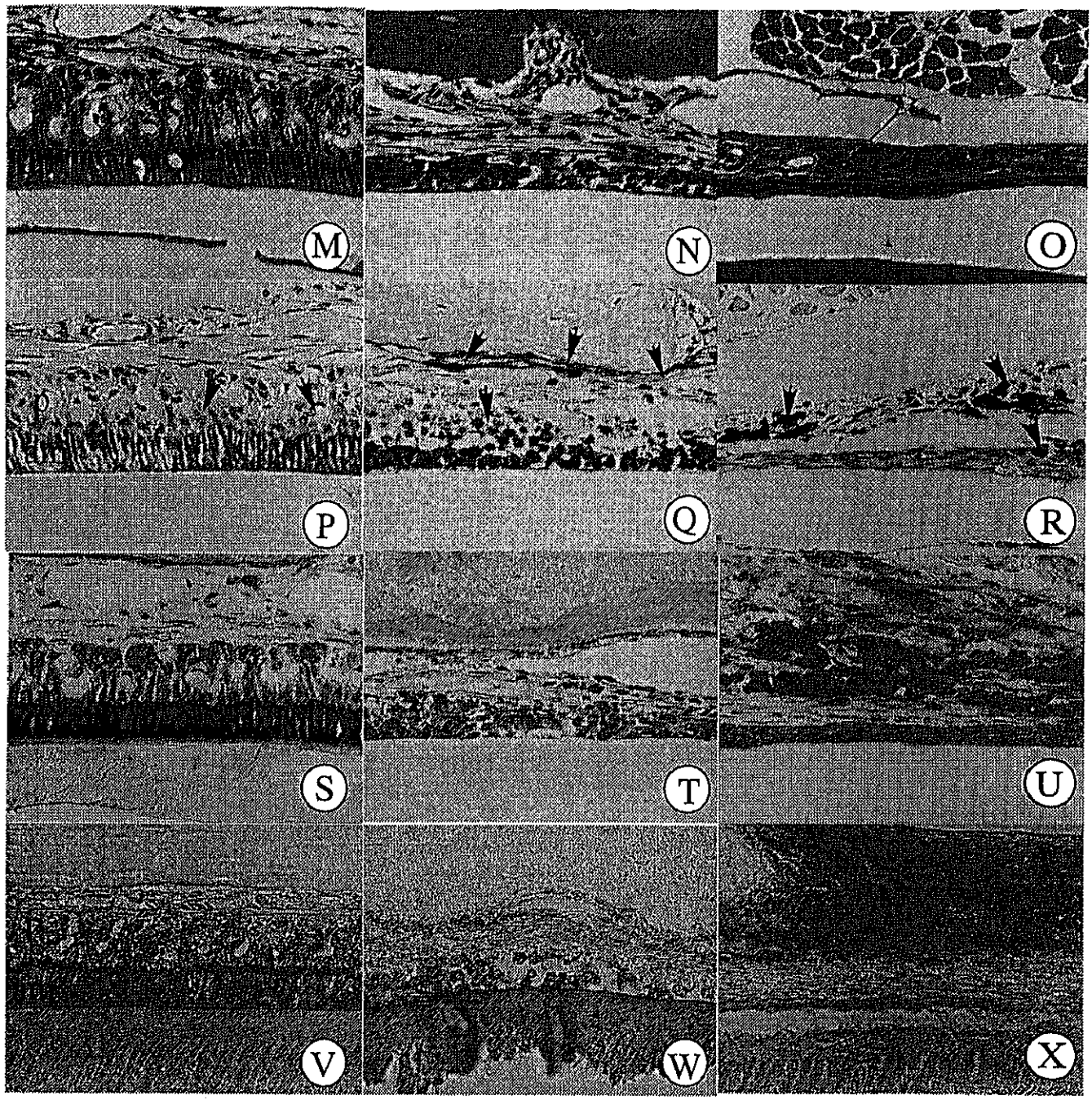
M
N
O
P
Q
R
S
T
U
V
W
X
Transition~early maturation stage
Late maturation stage
Region of reduced ameloblasts

Figure 4 (M-X)

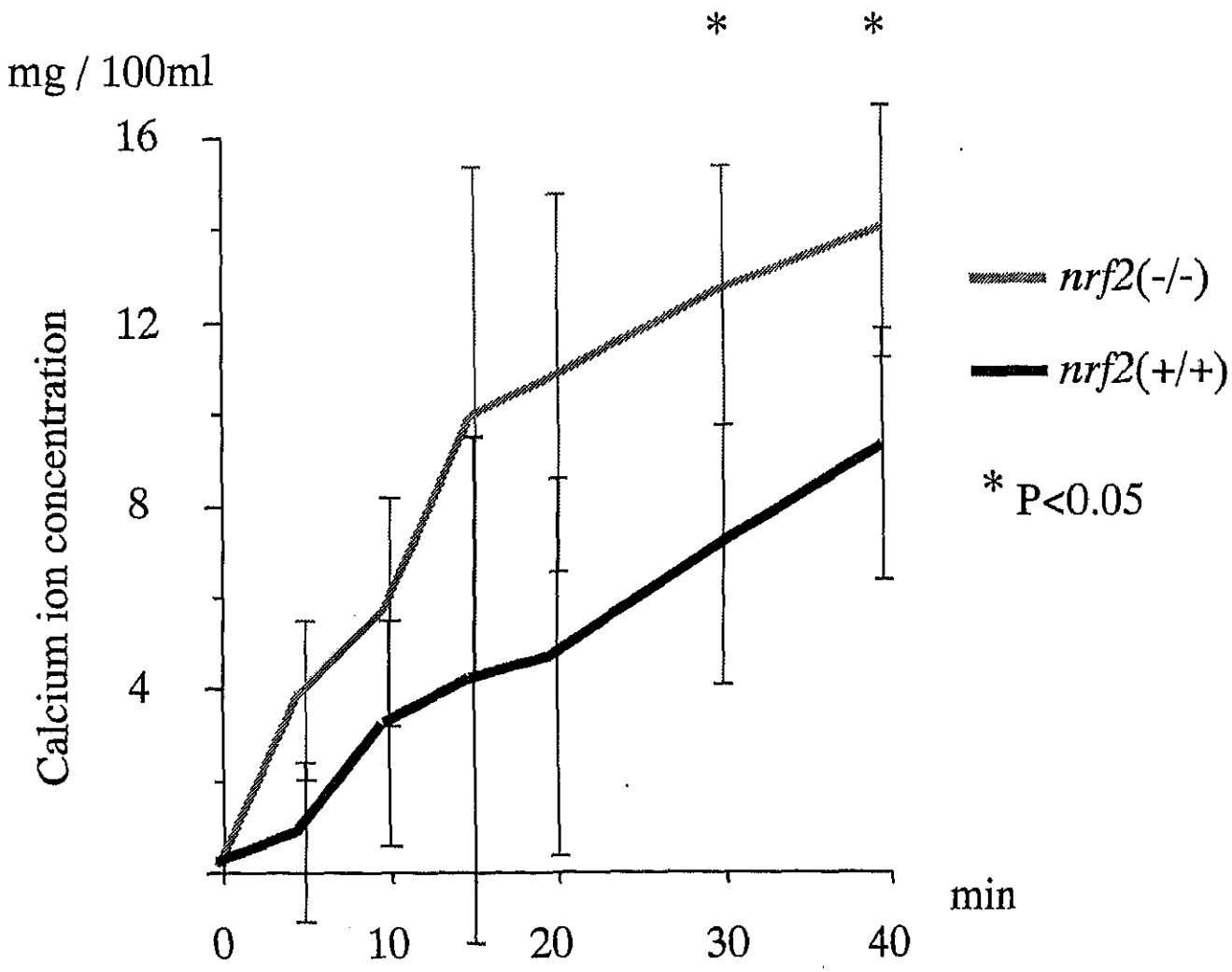
mg / 100ml
16
12
8
4
Calcium ion concentration
0
10
20
30
40
min
*
*
nrf2(-/-)
nrf2(+/+)
* P<0.05

Figure 5